

---

# Bridging Domain Gaps with Target-Aligned Generation for Offline Reinforcement Learning

---

Minung Kim      Jeongmo Kim      Gwanwoo Choi      Seungyul Han\*  
Graduate School of Artificial Intelligence  
Ulsan National Institute of Science and Technology (UNIST)  
{minungkim, jmkim22, cgw1999, syhan}@unist.ac.kr

## Abstract

Cross-domain offline reinforcement learning aims to adapt a policy from a source domain to a target domain using only pre-collected datasets, where environment dynamics may differ. A key challenge is to leverage source data while reducing distributional mismatch, particularly when the target dataset is extremely limited. To address this, we propose Target-aligned Coverage Expansion (TCE), a framework that decides how source data should be used, either by directly incorporating target-near transitions or by expanding state coverage through target-aligned generation, guided by theoretical analysis. TCE builds on a dual score-based generative model to synthesize target-consistent transitions over an expanded state region. Extensive experiments across diverse cross-domain environments show that TCE consistently outperforms state-of-the-art cross-domain offline RL baselines.

## 1 Introduction

Cross-domain reinforcement learning (cross-domain RL) aims to transfer a policy learned in a source domain to a target domain whose environment dynamics may differ. This setting arises in real-world applications such as heterogeneous robot control, simulation-to-real autonomous driving, and medical decision making [1, 2]. To address such scenarios, a variety of RL-based approaches have been proposed [3, 4]. However, most existing methods assume online interaction with the source or target domain, enabling additional data collection during training. In practice, this assumption often fails to hold due to cost and safety constraints, and in some cases online interaction is infeasible [5]. As a result, cross-domain offline RL, which uses only pre-collected datasets from both domains, has emerged as an important direction for cost-efficient learning without online interaction [6].

Early work on cross-domain offline RL primarily focused on selecting source-domain data similar to the target domain or filtering transitions via mutual-information criteria [7, 8], implicitly assuming that the target dataset is sufficiently large [9, 10]. When target data is abundant, single-domain offline RL algorithms such as CQL [11], IQL [12], and ReBRAC [13] often perform strongly, making additional source data unnecessary and sometimes detrimental. More recent work therefore considers a more challenging and realistic regime where the target dataset is extremely limited, and attempts to reduce the domain gap by leveraging source data that is close to the target domain [14, 15]. Nevertheless, when the gap between the source and target domains is large, directly incorporating source transitions can induce substantial distributional mismatch and degrade performance.

To address this challenge, we introduce Target-aligned Coverage Expansion (TCE), a method that reduces domain mismatch by controlling how source data is used, either through direct incorporation or target-aligned generation. Guided by theoretical analysis, TCE either incorporates target-near source transitions or uses them to expand state coverage via target-like transition generation. TCE builds on a dual score-based generative framework with stochastic differential equations (SDEs), consisting of a *mixture-state score network* trained on a controllable mixture of source and target states and a *target-transition score network* trained solely on target transitions. At inference time,

---

\*Corresponding Author

TCE constructs an augmented dataset by sampling mixture states and generating target-consistent next states conditioned on them. By jointly controlling source-data selection and the extent of coverage expansion, TCE limits mismatch introduced by augmentation while still benefiting from additional data. Empirically, TCE achieves substantial improvements over state-of-the-art cross-domain offline RL baselines across diverse cross-domain environments.

## 2 Related Works

**Cross-Domain Reinforcement Learning.** Early cross-domain RL methods allow online data collection and focus on learning domain-invariant representations or performing adversarial domain alignment to facilitate transfer [3, 16]. Cross-domain imitation learning extends this line by leveraging demonstrations across domains to generalize behavior without explicit rewards [4, 17, 18], while domain-adaptive imitation learning further addresses variations in environment dynamics [19]. However, many methods assume at least some level of online interaction or sufficiently large target data [20, 9, 10], limiting their applicability in purely offline settings. Offline cross-domain RL methods address this constraint [14] but remain challenged when the domain gap is large and target data is limited. To mitigate mismatch in this regime, recent work has explored optimal-transport-based selection [15], transition editing [21], source-data generation [22], robust test-time adaptation [23], and model-based target-dynamics learning [24]. In contrast, we generate target-aligned transitions from source data and, guided by theory, explicitly decide how such data should be utilized.

**Offline Reinforcement Learning.** Offline RL algorithms such as Conservative Q-Learning (CQL) [11] and Implicit Q-Learning (IQL) [12] have demonstrated strong performance in single-domain settings on static datasets such as the D4RL benchmark [25]. However, handling multi-domain data and domain shifts remains challenging [6, 26]. Filtering strategies based on mutual information [7, 8] and behavior regularization [13] have been used to mitigate distributional shift. Recently, diffusion-based techniques have shown promise in enabling effective data augmentation and model learning in offline RL, improving policy performance on limited datasets [27, 28]. In addition, Transformer-based methods have been proposed for offline learning in meta-RL settings [29].

**Score-Based Models and Diffusion Processes.** Two principal approaches to score-based generative modeling have enabled high-quality sample generation: denoising score matching, which estimates gradients of the data log-density across multiple noise scales [30, 31], and diffusion models, which progressively corrupt and then denoise data through a sequence of intermediate steps [32–34]. The stochastic differential equations (SDEs) framework unifies both approaches and enables principled continuous-time sampling [35, 36]. In this paper, we leverage the SDE formalism to learn a mixture state distribution and target dynamics from offline datasets, enabling controlled state-coverage expansion and the generation of target-aligned transitions for cross-domain offline RL.

## 3 Background

### 3.1 Cross-Domain Offline RL Setup

We define a Markov Decision Process (MDP) as  $\mathcal{M} = (\mathcal{S}, \mathcal{A}, P_{\mathcal{M}}, R, \gamma)$ , where  $\mathcal{S}$  is the state space,  $\mathcal{A}$  the action space,  $P_{\mathcal{M}}$  the transition dynamics,  $R$  the reward function, and  $\gamma$  the discount factor. In the cross-domain setting, we assume access to a source domain  $\mathcal{M}_{\text{src}} = (\mathcal{S}, \mathcal{A}, P_{\text{src}}, R, \gamma)$  and a target domain  $\mathcal{M}_{\text{tar}} = (\mathcal{S}, \mathcal{A}, P_{\text{tar}}, R, \gamma)$ , which share the same state and action spaces as well as the reward function but differ in their transition dynamics, i.e.,  $P_{\text{src}} \neq P_{\text{tar}}$ . In the cross-domain offline setting, the agent cannot interact with either domain and must rely solely on pre-collected transitions  $(s_t, a_t, r_t, s_{t+1})$ , where  $s_t \in \mathcal{S}$  denotes the state,  $a_t \in \mathcal{A}$  the action,  $r_t = R(s_t, a_t)$  the reward, and  $s_{t+1} \sim P(\cdot | s_t, a_t)$  the next state with  $P = P_{\text{src}}$  or  $P = P_{\text{tar}}$ . We denote the datasets collected from the source and target domains as  $\mathcal{D}_{\text{src}}$  and  $\mathcal{D}_{\text{tar}}$ , respectively, under the practical constraint that  $|\mathcal{D}_{\text{tar}}| \ll |\mathcal{D}_{\text{src}}|$ , making direct policy learning on the target domain challenging.

### 3.2 Score-based Generative Models with SDEs

Generative models aim to learn the data distribution  $p_{\text{data}}(x)$  and generate realistic samples. Representative approaches include Generative Adversarial Networks (GANs) [37], Variational Auto-Encoders (VAEs) [38], and diffusion models [32]. Among these, score-based generative models formulated with stochastic differential equations (SDEs) [35] provide a continuous-time view of diffusion, support flexible noise schedules, and enable efficient sampling and likelihood computation via the probability-flow ODE. Given a clean sample  $x^0$ , we perturb it with Gaussian noise as  $x^\tau = x^0 + \sigma(\tau)z$ , where

$z \sim \mathcal{N}(0, I)$ ,  $\tau \in [0, 1]$  denotes the continuous noise level, and  $\sigma(\tau)$  is the noise scale. In this paper, we consider a conditional input  $c$  and train a score network  $q_\theta(x, \tau | c)$  to estimate the conditional score  $\nabla_x \log p_\tau(x | c)$  via denoising score matching:

$$\mathcal{L}_{\text{score}}(\theta) = \mathbb{E}_{\tau, (x^0, c)} \left[ \zeta(\tau) \| q_\theta(x^\tau, \tau | c) + z/\sigma(\tau) \|_2^2 \right], \quad (1)$$

where  $\zeta(\tau)$  is a time-dependent weight. At sampling time, starting from  $x^1 \sim \mathcal{N}(0, \sigma(1)^2 I)$ , samples are generated by solving the discretized reverse SDE using the Predictor–Corrector sampler with discretized noise levels  $\tau^k$  ( $1 = \tau^K > \dots > \tau^0 = 0$ ):

$$x^{k-1} = x^k + [f(x^k, \tau^k) - g(\tau^k)^2 q_\theta(x^k, \tau^k | c)] \Delta\tau^k + g(\tau^k) \sqrt{|\Delta\tau^k|} \xi^k, \quad \xi^k \sim \mathcal{N}(0, I), \quad (2)$$

where  $f$  and  $g$  denote the drift and diffusion coefficients, and  $\Delta\tau^k = \tau^{k-1} - \tau^k$  is the step size. In this work, we additionally apply a Langevin corrector [30] after each predictor step to further improve sample quality. When the conditional input  $c$  is absent, the formulation simplifies to an unconditional score network  $q_\theta(x^\tau, \tau)$ . Implementation details for  $\zeta(\tau)$ ,  $f(x, \tau)$ ,  $g(\tau)$ , the step size  $\Delta\tau$ , and the Langevin corrector are provided in Appendix B.

## 4 Methodology

### 4.1 Beyond Source Data Selection in Cross-Domain Offline RL

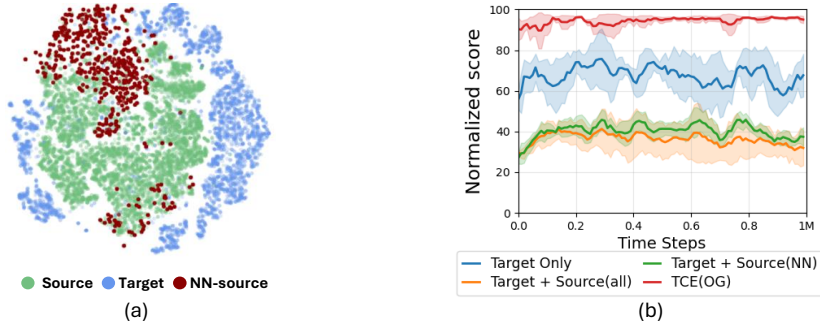


Figure 1: (a) t-SNE visualization of state transitions  $(s_t, s_{t+1})$  for the source, target, and NN-source sets. (b) offline RL performance on target-only, target+NN-source, target+source, and TCE. ‘TCE (OG)’ denotes a variant of TCE that uses only generated transitions without direct source use.

Most existing cross-domain offline RL methods address target-data scarcity by incorporating source-domain transitions that are closest to the target data under various distance metrics [14, 15], implicitly assuming that nearby source data improve target-domain learning. While such data can be beneficial, direct incorporation can degrade performance when the domain difference is large. To illustrate this, Fig. 1(a) presents a t-SNE visualization of state transitions  $(s_t, s_{t+1})$  from the source and target datasets in the MuJoCo Ant environment with different morphologies, revealing a substantial gap in their transition distributions. Following standard practice, we select nearest-neighbor (NN) source transitions of the target data (NN-source in Fig. 1(a)) and train IQL on three datasets: target-only, target+NN-source, and target+all source transitions. As shown in Fig. 1(b), both NN-selected and full-source augmentation perform worse than target-only training, indicating that naive source-data incorporation can hinder learning under large domain gaps.

This failure suggests that the key limitation lies in the direct use of source transitions under large source–target dynamics gaps, not merely in source-data selection. To address this, we introduce **Target-aligned Coverage Expansion (TCE)**, which goes beyond selecting target-near source data by leveraging source data for state-coverage expansion and generating transitions aligned with target dynamics. Our theoretical analysis decomposes the effective domain gap into two components: one from source–target dynamics differences and the other from generative model error due to limited target data. Based on this perspective, TCE controls how source data is used by determining how close source data should be and how far state coverage should be expanded so that neither component dominates. Accordingly, source data in TCE is used when it lies near the target distribution or contributes to target-aligned coverage expansion. Consistent with this design, Fig. 1(b) illustrates that different regimes favor different uses of source data, where target-aligned generation is more appropriate under large dynamics gaps, while direct incorporation of selected source data can be effective when the gap is smaller.

## 4.2 Theoretical Analysis

In this section, we present TCE, which controls how source data is used through either direct utilization or state-coverage expansion via generation. For an MDP  $\mathcal{M}$  and policy  $\pi$ , let the occupancy measure be  $\rho_{\mathcal{M}}^{\pi}(s, a) := (1 - \gamma) \sum_{t=0}^{\infty} \gamma^t P_{\mathcal{M}}(s | s_t, a) \pi(a | s_t)$ , the value function  $V_{\mathcal{M}}^{\pi}(s_t) = \mathbb{E}_{\rho_{\mathcal{M}}^{\pi}} [\sum_{l=t}^{\infty} \gamma^l r(s_l, a_l)]$ , and the average return  $\eta_{\mathcal{M}}(\pi) = \mathbb{E}_{\rho_{\mathcal{M}}^{\pi}} [r(s, a)]$ . Our goal is to maximize the target return  $\eta_{\text{tar}}(\pi)$  using both  $\mathcal{D}_{\text{tar}}$  and  $\mathcal{D}_{\text{src}}$ .

To capture the two ways TCE leverages source information, let  $P_{\text{src}}$  denote the source transition and  $\hat{P}_{\text{tar}}$  an approximate target transition induced by generation. We consider their mixture  $P_{\text{mix}} = \lambda P_{\text{src}} + (1 - \lambda) \hat{P}_{\text{tar}}$ ,  $\lambda \in [0, 1]$ , and denote the induced MDP by  $\mathcal{M}_{\text{mix}}$ . Under this construction, the following theoretical gap bound holds, modified from Xu et al. [9].

**Theorem 4.1.** *Let  $\eta_{\text{mix}}(\pi)$  and  $\rho_{\text{mix}}^{\pi}$  denote the expected return and the state-action occupancy measure in the mixture MDP, respectively. Then, the performance gap between the target MDP and the mixture MDP can be bounded in terms of transition dynamics as follows:*

$$\eta_{\text{mix}}(\pi) - \eta_{\text{tar}}(\pi) \leq \frac{2\gamma r_{\max}}{(1 - \gamma)^2} \left( \lambda \mathbb{E}_{\rho_{\text{mix}}^{\pi}} [D_{\text{TV}}(P_{\text{src}} \| P_{\text{tar}})] + (1 - \lambda) \mathbb{E}_{\rho_{\text{mix}}^{\pi}} [D_{\text{TV}}(\hat{P}_{\text{tar}} \| P_{\text{tar}})] \right), \quad (3)$$

where  $r_{\max}$  denotes the maximum reward and  $D_{\text{TV}}(P \| Q)$  denotes the total variation distance between  $P$  and  $Q$ .

**Proof)** Proof of Theorem 4.1 is provided in Appendix A.

From Theorem 4.1, the gap can be reduced in two complementary ways: (1) minimizing the dynamics gap  $D_{\text{TV}}(P_{\text{src}} \| P_{\text{tar}})$  by selecting source data close to the target distribution, and (2) reducing the generation error  $D_{\text{TV}}(\hat{P}_{\text{tar}} \| P_{\text{tar}})$  by improving model fidelity. TCE jointly controls both factors.

## 4.3 State Coverage Expansion with Score-Based Generative Models

As discussed in the motivation, when the dynamics gap is large, TCE leverages source data to expand target-state coverage by generating target-aligned transitions. To this end, we introduce two score networks: a *mixture-state score network*  $q_{\theta}^{\text{mix}}$  for a mixture of source and target states, and a *target-transition score network*  $q_{\theta}^{\text{tran}}$  for generating target-like transitions conditioned on them. Since  $q_{\theta}^{\text{tran}}$  is trained only on target transitions, its error grows for inputs far from target support. We therefore restrict the mixture to source samples near the target using a nearest-neighbor (NN) criterion.

Specifically, for a source transition  $(s, s') \in \mathcal{D}_{\text{src}}$ , define the NN distance to the target set as  $d_{\text{NN}}(s, s') := \min_{(\tilde{s}, \tilde{s}') \in \mathcal{D}_{\text{tar}}} \|s - \tilde{s}\| + \|s' - \tilde{s}'\|$ . Let  $\lambda_{\text{cov}} \in [0, 1]$  be a coverage coefficient, and let  $d_{\lambda_{\text{cov}}}$  be the corresponding quantile threshold. The selected subset is

$$\mathcal{D}_{\text{src}}^{\lambda_{\text{cov}}} := \{(s, s') \in \mathcal{D}_{\text{src}} : d_{\text{NN}}(s, s') \leq d_{\lambda_{\text{cov}}}\}. \quad (4)$$

We train  $q_{\theta}^{\text{mix}}$  on  $\mathcal{D}_{\text{src}}^{\lambda_{\text{cov}}} \cup \mathcal{D}_{\text{tar}}$ , where  $\lambda_{\text{cov}}$  controls the trade-off between coverage expansion and generation error. When  $\lambda_{\text{cov}} = 0$ , the model reduces to target-only training; as  $\lambda_{\text{cov}}$  increases, coverage expands at the cost of higher generation error.

Building on the score-based framework in Eq. (1), we jointly train the two score networks with

$$\underbrace{\mathbb{E}_{\tau, s_t \sim \mathcal{D}_{\text{src}}^{\lambda_{\text{cov}}} \cup \mathcal{D}_{\text{tar}}} \left[ \zeta(\tau) \left\| q_{\theta}^{\text{mix}}(s_t^{\tau}, \tau) + \frac{z}{\sigma(\tau)} \right\|_2^2 \right]}_{\text{mixture-state score network loss}} + \underbrace{\mathbb{E}_{\tau, (s_t, s_{t+1}) \sim \mathcal{D}_{\text{tar}}} \left[ \zeta(\tau) \left\| q_{\theta}^{\text{tran}}(s_{t+1}^{\tau}, \tau | s_t) + \frac{z}{\sigma(\tau)} \right\|_2^2 \right]}_{\text{target-transition score network loss}} \quad (5)$$

where  $z \sim \mathcal{N}(0, I)$  and  $s^{\tau} = \alpha(\tau)s + \sigma(\tau)z$ . The mixture-state network models the expanded state distribution, while the transition network generates target-consistent next states. We measure NN distance using  $(s, s')$  so that the same transition-level criterion governs both source reuse and the control of dynamics and generation gaps.

**Auxiliary Models.** To construct full transitions aligned with target dynamics, we train an inverse dynamics model  $\text{Inv}_{\psi}$  and a reward model  $\hat{R}_{\phi}$ . The inverse model predicts the action from a state transition  $(s, s')$  and is trained on  $\mathcal{D}_{\text{tar}}$ , ensuring consistency with target dynamics. The reward model predicts the reward and is trained on  $\mathcal{D}_{\text{src}} \cup \mathcal{D}_{\text{tar}}$ , as the reward function is shared across domains.

After training, we generate transition samples with a two-stage procedure based on Eq. (2) as follows.

**Stage 1 (State Sampling):** Starting from Gaussian noise  $s^K \sim \mathcal{N}(0, I)$ , we integrate the reverse SDE backward from  $k = K$  to 0 using the mixture-based score network:

$$s^{k-1} = s^k + \left[ f(s^k, \tau^k) - g(\tau^k)^2 q_{\theta}^{\text{mix}}(s^k, \tau^k) \right] \Delta\tau^k + g(\tau^k) \sqrt{|\Delta\tau^k|} \xi^k, \quad \xi^k \sim \mathcal{N}(0, I), \quad (6)$$

where  $f$  and  $g$  denote the drift and diffusion coefficients, and  $s^0$  corresponds to the generated state  $\hat{s}_t$ .

**Stage 2 (Transition Sampling):** Conditioned on  $\hat{s}_t$ , we obtain its next state  $\hat{s}_{t+1}$  by solving the same reverse SDE using the target-transition score network:

$$s^{k-1} = s^k + \left[ f(s^k, \tau^k) - g(\tau^k)^2 q_{\theta}^{\text{tran}}(s^k, \tau^k \mid \hat{s}_t) \right] \Delta\tau^k + g(\tau^k) \sqrt{|\Delta\tau^k|} \xi^k, \quad \xi^k \sim \mathcal{N}(0, I), \quad (7)$$

again integrating from  $k = K$  to 0 to yield  $\hat{s}_{t+1} = s^0$ . The resulting pair  $(\hat{s}_t, \hat{s}_{t+1})$  forms a transition that expands the support of the target dataset while remaining consistent with target dynamics. We then form the full transition  $(\hat{s}_t, \hat{a}_t, \hat{r}_t, \hat{s}_{t+1})$  by recovering the action and reward using the auxiliary models,  $\hat{a}_t \sim \text{Inv}_{\psi}(\hat{s}_t, \hat{s}_{t+1})$  and  $\hat{r}_t \sim \hat{R}_{\phi}(\hat{s}_t, \hat{a}_t, \hat{s}_{t+1})$ , and denote the resulting dataset as  $\mathcal{D}_{\text{gen}}^{\lambda_{\text{cov}}}$ .

We adopt this two-stage design instead of directly learning a state-action mixture model for next-state prediction, as the target dataset is often limited and provides too few next-state samples per state-action pair for reliable generalization. Consequently, directly learning  $\hat{P}_{\text{tar}}(s' \mid s, a)$  can overfit and introduce large errors even under the same state-coverage expansion, destabilizing training. In contrast, by decoupling state coverage expansion and transition modeling, our approach enables more stable generalization from limited target data, which we validate empirically.

#### 4.4 Training Dataset Construction and Offline Policy Learning

We next construct a training dataset that reflects the mixture MDP analysis using the generated transitions  $\mathcal{D}_{\text{gen}}^{\lambda_{\text{cov}}}$ . Recall that in Theorem 4.1, the mixture MDP is induced by combining source transitions  $P_{\text{src}}$  and generated target-like transitions  $\hat{P}_{\text{tar}}$ . Since the occupancy measure  $\rho_{\text{mix}}^{\pi}$  is intractable, we approximate this mixture by combining real source transitions with  $\mathcal{D}_{\text{gen}}^{\lambda_{\text{cov}}}$ .

Because directly using source transitions introduces a dynamics gap measured by  $D_{\text{TV}}(P_{\text{src}} \parallel P_{\text{tar}})$ , we control their contribution via a *mixture coefficient*  $\lambda_{\text{mix}} \in [0, 1]$ , selecting target-near source transitions using the same NN criterion as in Eq. (4). We denote the resulting subset by  $\mathcal{D}_{\text{src}}^{\lambda_{\text{mix}}}$  and form the final training dataset as

$$\mathcal{D}_{\text{train}} = \mathcal{D}_{\text{src}}^{\lambda_{\text{mix}}} \cup \mathcal{D}_{\text{gen}}^{\lambda_{\text{cov}}} \cup \mathcal{D}_{\text{tar}}.$$

Here,  $\lambda_{\text{mix}}$  determines whether and how source transitions are used directly, while  $\lambda_{\text{cov}}$  controls the extent of generation-based coverage expansion.

	Method	Hyperparams
$\lambda_{\text{cov}} > 0$	(a) TCE (OG)	$\lambda_{\text{cov}} \in (0, 1]$ $\lambda_{\text{mix}} = 0$
	(b)	$\lambda_{\text{cov}} \in [0, 1]$ $\lambda_{\text{mix}} \in (0, 1]$
$\lambda_{\text{cov}} = 0$	(c) Simple Aug.	$\lambda_{\text{cov}} = 0$ $\lambda_{\text{mix}} = 0$

Figure 2: Classification of TCE variants.

for generation-based coverage expansion (**TCE(OG)**). When  $\lambda_{\text{mix}} > 0$ , target-near source transitions are additionally incorporated (**TCE(SM)**). Selecting a  $\lambda_{\text{mix}}$  fraction of the source dataset yields  $|\mathcal{D}_{\text{src}}^{\lambda_{\text{mix}}}| = \lambda_{\text{mix}} |\mathcal{D}_{\text{src}}|$  by construction, with the remaining transitions generated.

Using  $\mathcal{D}_{\text{train}}$ , we perform offline policy learning. We adopt Implicit Q-Learning (IQL) for fair comparison with prior work [12], and follow Lyu et al. [15] to incorporate a KL regularization term that penalizes deviation from the target-domain behavior policy. The resulting objective is

$$\mathcal{L}_{\pi} = \mathcal{L}_{\pi}^{\text{IQL}} + \beta \mathbb{E}_{s \sim \mathcal{D}_{\text{tar}}} [D_{\text{KL}}(\hat{\pi}_{\text{b}}(\cdot \mid s) \parallel \pi(\cdot \mid s))], \quad (8)$$

where  $\hat{\pi}_{\text{b}}$  is the empirical behavior policy estimated from the target dataset. The overall framework of TCE is illustrated in Fig. 3, and the full procedure is summarized in Algorithm 1. Further implementation details are provided in Appendix B.

In summary,  $\lambda_{\text{cov}}$  regulates the generation error term  $D_{\text{TV}}(\hat{P}_{\text{tar}} \parallel P_{\text{tar}})$  by controlling state-coverage expansion, while  $\lambda_{\text{mix}}$  controls the dynamics gap  $D_{\text{TV}}(P_{\text{src}} \parallel P_{\text{tar}})$  by determining the amount of source data directly incorporated. Fig. 2 summarizes the resulting variants of TCE. When  $\lambda_{\text{cov}} = \lambda_{\text{mix}} = 0$ , TCE reduces to target-only generation (**Simple Augmentation**). When  $\lambda_{\text{mix}} = 0$  and  $\lambda_{\text{cov}} > 0$ , source data is used only

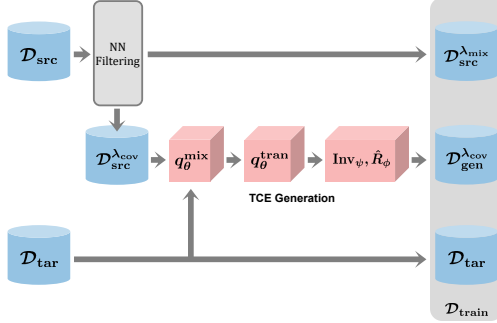


Figure 3: Data construction in TCE framework.

---

### Algorithm 1 TCE Framework

---

- 1: **Input:**  $\mathcal{D}_{\text{tar}}, \mathcal{D}_{\text{src}}, \lambda_{\text{cov}}, \lambda_{\text{mix}}$
  - 2: **Train models:** Train  $q_{\theta}^{\text{mix}}$  on  $\mathcal{D}_{\text{src}}^{\lambda_{\text{cov}}} \cup \mathcal{D}_{\text{tar}}$ ,
  - 3: and  $q_{\theta}^{\text{tran}}$  on  $\mathcal{D}_{\text{tar}}$  via Eq. (5)
  - 4: Train  $\text{Inv}_{\psi}$  on  $\mathcal{D}_{\text{tar}}$ , and  $\hat{R}_{\phi}$  on  $\mathcal{D}_{\text{src}} \cup \mathcal{D}_{\text{tar}}$
  - 5: **Generate samples:**
  - 6: Generate  $\hat{s}_t \sim q_{\theta}^{\text{mix}}, \hat{s}_{t+1} \sim q_{\theta}^{\text{tran}}(\cdot | \hat{s}_t)$ ,
  - 7:  $\hat{a}_t \sim \text{Inv}_{\psi}$ , and  $\hat{r}_t \sim \hat{R}_{\phi}$  to form  $\mathcal{D}_{\text{gen}}^{\lambda_{\text{cov}}}$
  - 8: **Construct training data:**
  - 9:  $\mathcal{D}_{\text{train}} = \mathcal{D}_{\text{gen}}^{\lambda_{\text{cov}}} \cup \mathcal{D}_{\text{tar}}$  (**TCE(OG)**)
  - 10:  $\mathcal{D}_{\text{train}} = \mathcal{D}_{\text{src}}^{\lambda_{\text{mix}}} \cup \mathcal{D}_{\text{gen}}^{\lambda_{\text{cov}}} \cup \mathcal{D}_{\text{tar}}$  (**TCE(SM)**)
  - 11: **Offline RL:** Train  $\pi$  on the training dataset  $\mathcal{D}_{\text{train}}$
- 

## 5 Experiments

In this section, we evaluate TCE across diverse cross-domain setups and compare it with recent cross-domain offline RL baselines. We further perform ablations to quantify the contribution of each component and study sensitivity to key hyperparameters.

### 5.1 Experimental Setup

We evaluate TCE on cross-domain MuJoCo continuous-control tasks [39] and Adroit manipulation tasks from the ODRL benchmark [40]. In MuJoCo, the source and target domains share the same agent type (HalfCheetah, Hopper, Walker2d, Ant) but differ in morphology, kinematics, or gravity. Both domains use pre-collected D4RL datasets [25] with varying quality: for the target domain, we consider medium, medium-expert, and expert, while for the source domain we use medium, medium-replay, and medium-expert. This yields 36 cross-domain tasks for each of the morphology-, kinematics-, and gravity-shift settings, with approximately 0.2M–2M source transitions and 5k target transitions. In Adroit, we consider morphology (shrink-finger) and kinematic (broken-joint) shifts, using expert-only source and target datasets with 0.5M source transitions and 5k target transitions; M/H denote medium and hard shift levels corresponding to stronger physical constraints in the target domain. We report normalized returns, where 0 corresponds to a random policy and 100 to an expert policy. Further environmental details are provided in Appendix C.

For comparison on MuJoCo tasks, we evaluate TCE variants against a comprehensive set of cross-domain offline RL baselines: **IQL\*** [12], which trains IQL on the union of source and target data; **DARA** [6], which employs domain-adversarial classifiers to mitigate dynamics mismatch; **BOSA** [26], which constrains the policy to the support of the dataset; **SRPO** [41], which regularizes policy learning by matching stationary distributions; **IGDF** [14], which filters source transitions using representation learning; and **OTDF** [15], which performs source filtering based on optimal transport distances. For Adroit, we use the official ODRL benchmark [40] and additionally compare against **MOBODY** [24], a model-based adaptation baseline, in place of SRPO, whose official implementation does not support Adroit environments.

For the baseline methods, we report results directly from [15], where each algorithm is implemented with hyperparameter tuning. For TCE variants, we consider **TCE(OG)** and **TCE(SM)**: for both variants we select the best  $\lambda_{\text{cov}} \in (0, 1]$ , and for TCE(SM) we additionally tune  $\lambda_{\text{mix}} \in (0, 1]$  via hyperparameter search. All TCE variants are trained for the same number of steps as the baselines. More details, including hyperparameter settings, are provided in Appendix C.

### 5.2 Performance Comparison

**Morphology Shifts.** Table 1 summarizes the results under morphology shifts. TCE achieves the highest average performance on 33 of 36 tasks, outperforming all baselines. The gains are most pronounced when the target dataset is high-quality (e.g., expert), where many baselines fail due to the narrow target distribution and large domain gap. By combining controllable state-coverage expansion with target-aligned transition generation, TCE effectively mitigates distributional shift and enables offline policy learning in these challenging settings. Morphology shifts induce the largest

Table 1: Performance comparison on morphology-shift tasks. Abbrev.: half=HalfCheetah, hopp=Hopper, walk=Walker2d, ant=Ant; m=medium, m-r=medium-replay, e=expert, m-e=medium-expert. Src./Tgt. denote source/target domains. Results are reported as mean  $\pm$  standard deviation over 5 seeds; best results are in **bold** and second-best results are underlined.

Src.	Tgt.	IQL*	DARA	BOSA	SRPO	IGDF	OTDF	TCE(OG)	TCE(SM)
half-m	m	30.0 $\pm$ 1.6	26.6 $\pm$ 3.3	19.3 $\pm$ 3.5	41.3 $\pm$ 0.4	41.6 $\pm$ 0.5	39.1 $\pm$ 2.3	<b>44.1<math>\pm</math>0.2</b>	<b>44.1<math>\pm</math>0.2</b>
half-m	m-e	31.8 $\pm$ 1.1	32.0 $\pm$ 0.7	33.6 $\pm$ 1.1	30.7 $\pm$ 0.8	29.6 $\pm$ 2.2	35.6 $\pm$ 0.7	<b>44.7<math>\pm</math>0.6</b>	<u>43.3<math>\pm</math>0.5</u>
half-m	e	8.5 $\pm$ 1.0	9.3 $\pm$ 1.6	7.9 $\pm$ 0.8	8.6 $\pm$ 0.9	10.0 $\pm$ 0.8	10.7 $\pm$ 1.2	<b>81.7<math>\pm</math>9.2</b>	<u>61.5<math>\pm</math>4.5</u>
half-m-r	m	30.8 $\pm$ 4.4	35.6 $\pm$ 0.7	35.0 $\pm$ 4.6	32.0 $\pm$ 1.4	28.0 $\pm$ 2.0	40.0 $\pm$ 1.2	<b>44.2<math>\pm</math>1.0</b>	<u>43.3<math>\pm</math>2.3</u>
half-m-r	m-e	12.9 $\pm$ 2.2	16.9 $\pm$ 4.1	19.9 $\pm$ 5.5	12.4 $\pm$ 1.6	12.0 $\pm$ 3.7	34.4 $\pm$ 0.7	<b>44.2<math>\pm</math>1.3</b>	<u>43.1<math>\pm</math>0.1</u>
half-m-r	e	5.9 $\pm$ 1.7	3.7 $\pm$ 2.7	2.4 $\pm$ 1.9	6.2 $\pm$ 1.4	5.3 $\pm$ 2.3	8.2 $\pm$ 2.7	<b>80.2<math>\pm</math>0.8</b>	<u>36.9<math>\pm</math>8.6</u>
half-m-e	m	41.5 $\pm$ 0.1	40.3 $\pm$ 1.2	41.3 $\pm$ 0.3	41.3 $\pm$ 0.4	40.9 $\pm$ 0.4	41.4 $\pm$ 0.3	<b>44.1<math>\pm</math>1.3</b>	<b>44.1<math>\pm</math>2.0</b>
half-m-e	m-e	25.8 $\pm$ 2.0	30.6 $\pm$ 2.8	32.1 $\pm$ 0.8	27.2 $\pm$ 0.8	26.2 $\pm$ 1.8	35.1 $\pm$ 0.6	<b>44.8<math>\pm</math>0.5</b>	<u>43.8<math>\pm</math>2.0</u>
half-m-e	e	7.8 $\pm$ 1.3	8.3 $\pm$ 1.3	9.1 $\pm$ 0.8	7.8 $\pm$ 0.9	7.5 $\pm$ 0.9	9.8 $\pm$ 1.0	<b>83.2<math>\pm</math>5.1</b>	<u>62.9<math>\pm</math>8.3</u>
hopp-m	m	<u>13.5<math>\pm</math>0.2</u>	<u>13.5<math>\pm</math>0.4</u>	13.2 $\pm$ 0.3	13.4 $\pm$ 0.1	13.4 $\pm$ 0.2	11.0 $\pm$ 0.9	<b>50.0<math>\pm</math>2.0</b>	5.0 $\pm$ 3.7
hopp-m	m-e	<u>13.4<math>\pm</math>0.1</u>	<u>13.6<math>\pm</math>0.2</u>	11.2 $\pm$ 4.6	13.3 $\pm$ 0.2	13.3 $\pm$ 0.4	12.6 $\pm$ 0.8	<b>16.1<math>\pm</math>5.3</b>	9.2 $\pm$ 1.8
hopp-m	e	13.5 $\pm$ 0.2	13.6 $\pm$ 0.3	13.3 $\pm$ 0.4	13.6 $\pm$ 0.2	13.9 $\pm$ 0.1	10.7 $\pm$ 4.7	<b>99.8<math>\pm</math>0.1</b>	<u>77.3<math>\pm</math>15.7</u>
hopp-m-r	m	10.8 $\pm$ 1.1	10.2 $\pm$ 1.0	1.2 $\pm$ 0.0	10.7 $\pm$ 1.6	12.0 $\pm$ 4.4	8.7 $\pm$ 2.8	<b>31.1<math>\pm</math>3.2</b>	<u>27.0<math>\pm</math>14.5</u>
hopp-m-r	m-e	11.6 $\pm$ 1.6	10.4 $\pm$ 0.9	1.3 $\pm$ 0.2	10.4 $\pm$ 1.2	8.2 $\pm$ 2.8	9.7 $\pm$ 2.7	<b>15.8<math>\pm</math>4.1</b>	3.4 $\pm$ 0.1
hopp-m-r	e	9.8 $\pm$ 0.5	9.0 $\pm$ 0.3	1.3 $\pm$ 0.1	10.4 $\pm$ 1.4	11.4 $\pm$ 1.5	10.7 $\pm$ 2.4	<b>99.8<math>\pm</math>0.1</b>	<u>75.4<math>\pm</math>26.1</u>
hopp-m-e	m	12.6 $\pm$ 1.4	13.0 $\pm$ 0.5	15.7 $\pm$ 7.2	14.0 $\pm$ 2.3	12.7 $\pm$ 0.8	7.9 $\pm$ 3.2	<b>50.5<math>\pm</math>7.6</b>	<u>22.0<math>\pm</math>17.3</u>
hopp-m-e	m-e	<u>14.1<math>\pm</math>1.3</u>	13.8 $\pm$ 0.6	12.0 $\pm$ 1.4	13.5 $\pm$ 0.3	13.3 $\pm$ 1.2	9.6 $\pm$ 3.5	<b>18.8<math>\pm</math>6.5</b>	<u>10.2<math>\pm</math>1.3</u>
hopp-m-e	e	13.8 $\pm$ 0.5	12.3 $\pm$ 1.8	10.5 $\pm$ 5.0	14.7 $\pm$ 2.3	12.8 $\pm$ 0.9	5.9 $\pm$ 4.0	<b>97.9<math>\pm</math>0.3</b>	<u>66.1<math>\pm</math>23.1</u>
walk-m	m	23.0 $\pm$ 4.7	23.3 $\pm$ 3.3	6.2 $\pm$ 2.9	24.7 $\pm$ 1.7	27.5 $\pm$ 9.5	50.5 $\pm$ 5.8	43.2 $\pm$ 3.8	<b>55.2<math>\pm</math>5.3</b>
walk-m	m-e	21.5 $\pm$ 8.6	22.2 $\pm$ 7.6	7.2 $\pm$ 2.9	18.7 $\pm$ 7.3	20.7 $\pm$ 5.9	<b>44.3<math>\pm</math>23.8</b>	40.4 $\pm$ 2.5	22.7 $\pm$ 9.7
walk-m	e	20.3 $\pm$ 2.8	17.3 $\pm$ 3.4	15.8 $\pm$ 8.7	21.1 $\pm$ 7.2	15.8 $\pm$ 4.5	55.3 $\pm$ 8.3	<u>74.2<math>\pm</math>1.6</u>	<b>86.8<math>\pm</math>11.8</b>
walk-m-r	m	11.3 $\pm$ 3.0	10.9 $\pm$ 4.6	5.4 $\pm$ 4.0	10.4 $\pm$ 4.8	13.4 $\pm$ 7.2	37.4 $\pm$ 5.1	<u>44.7<math>\pm</math>2.7</u>	<b>45.6<math>\pm</math>10.4</b>
walk-m-r	m-e	7.0 $\pm$ 1.5	4.5 $\pm$ 1.1	4.0 $\pm$ 2.2	4.9 $\pm$ 1.7	6.9 $\pm$ 2.2	33.8 $\pm$ 6.9	<b>43.4<math>\pm</math>2.6</b>	17.2 $\pm$ 3.1
walk-m-r	e	6.3 $\pm$ 0.9	4.5 $\pm$ 1.1	3.8 $\pm$ 3.4	5.5 $\pm$ 0.9	5.5 $\pm$ 2.2	41.5 $\pm$ 6.8	<b>63.2<math>\pm</math>7.4</b>	<u>52.6<math>\pm</math>0.2</u>
walk-m-e	m	24.1 $\pm$ 7.4	31.7 $\pm$ 6.6	18.7 $\pm$ 6.5	29.9 $\pm$ 4.7	27.5 $\pm$ 2.3	<b>49.9<math>\pm</math>4.6</b>	43.5 $\pm$ 3.4	<u>47.4<math>\pm</math>3.6</u>
walk-m-e	m-e	27.0 $\pm$ 5.5	23.3 $\pm$ 5.5	11.1 $\pm$ 0.9	22.9 $\pm$ 3.8	25.3 $\pm$ 6.4	<b>40.5<math>\pm</math>11.0</b>	<u>37.4<math>\pm</math>6.1</u>	21.7 $\pm$ 7.9
walk-m-e	e	22.4 $\pm$ 3.3	25.2 $\pm$ 5.7	9.9 $\pm$ 3.9	18.7 $\pm$ 5.7	24.7 $\pm$ 2.4	45.7 $\pm$ 6.9	<b>62.5<math>\pm</math>9.6</b>	<u>47.6<math>\pm</math>10.9</u>
ant-m	m	38.7 $\pm$ 3.8	41.3 $\pm$ 1.8	18.2 $\pm$ 1.9	40.6 $\pm$ 2.1	40.9 $\pm$ 1.7	39.4 $\pm$ 1.7	<b>41.5<math>\pm</math>0.8</b>	40.8 $\pm$ 1.2
ant-m	m-e	47.0 $\pm$ 5.1	43.3 $\pm$ 2.0	45.3 $\pm$ 7.0	47.2 $\pm$ 4.3	44.4 $\pm$ 1.7	58.3 $\pm$ 8.9	<u>72.7<math>\pm</math>2.5</u>	<b>74.9<math>\pm</math>4.0</b>
ant-m	e	36.2 $\pm$ 3.5	48.5 $\pm$ 4.2	72.2 $\pm$ 10.5	42.2 $\pm$ 9.9	41.4 $\pm$ 4.2	85.4 $\pm$ 4.4	<u>94.0<math>\pm</math>4.5</u>	<b>96.4<math>\pm</math>3.2</b>
ant-m-r	m	38.2 $\pm$ 2.9	38.9 $\pm$ 2.7	20.2 $\pm$ 3.7	38.3 $\pm$ 1.9	39.7 $\pm$ 1.2	41.2 $\pm$ 0.9	<b>41.5<math>\pm</math>1.5</b>	40.0 $\pm$ 1.6
ant-m-r	m-e	38.1 $\pm$ 3.5	33.4 $\pm$ 5.5	15.2 $\pm$ 1.6	35.0 $\pm$ 5.7	37.3 $\pm$ 2.4	50.8 $\pm$ 4.5	<b>71.0<math>\pm</math>8.4</b>	<u>63.1<math>\pm</math>9.8</u>
ant-m-r	e	24.1 $\pm$ 1.9	24.5 $\pm$ 2.6	16.0 $\pm$ 1.7	22.7 $\pm$ 3.0	23.6 $\pm$ 1.4	67.2 $\pm$ 7.5	<b>96.1<math>\pm</math>0.4</b>	<b>96.1<math>\pm</math>0.6</b>
ant-m-e	m	32.9 $\pm$ 5.1	40.2 $\pm$ 1.5	28.1 $\pm$ 5.6	35.9 $\pm$ 2.5	36.1 $\pm$ 4.4	39.9 $\pm$ 2.9	<b>41.9<math>\pm</math>0.6</b>	41.4 $\pm$ 1.8
ant-m-e	m-e	35.7 $\pm$ 3.9	36.5 $\pm$ 8.7	14.8 $\pm$ 15.9	24.5 $\pm$ 15.7	30.7 $\pm$ 10.8	65.7 $\pm$ 4.5	<u>66.4<math>\pm</math>1.2</u>	<b>69.2<math>\pm</math>4.9</b>
ant-m-e	e	36.1 $\pm$ 8.5	34.6 $\pm$ 5.8	53.9 $\pm$ 5.0	38.4 $\pm$ 9.4	35.2 $\pm$ 6.6	86.4 $\pm$ 2.2	<b>96.6<math>\pm</math>0.5</b>	<u>94.5<math>\pm</math>2.4</u>
<b>Total Score</b>		798.0	816.8	646.3	803.1	808.7	1274.3	<b>2065.2</b>	<u>1731.8</u>

domain gaps, as structural changes in the agent substantially alter both the state distribution and transition dynamics. In this regime, TCE(OG) consistently performs best, while TCE(SM) is effective only with small mixing weights and can degrade performance even with slight source incorporation, indicating that generation is more effective than direct mixing under large gaps.

**Kinematic Shifts & Gravity Shifts.** We defer full results to Appendix D.1 and D.2, as each setup involves 36 tasks. Kinematic shifts modify transition dynamics through changes in kinematic parameters and generally induce larger gaps than gravity shifts. Consistent with this, TCE outperforms baselines on nearly all tasks, with TCE(OG) remaining the strongest variant in most cases. In contrast, gravity shifts alter vertical dynamics while preserving the overall agent structure, resulting in a milder domain gap. In this regime, TCE(SM) surpasses both TCE(OG) and the baselines, indicating that incorporating target-near source transitions becomes more beneficial as the gap decreases. This trend is further confirmed in the *extreme-shift* study in Appendix D.3, where TCE(OG) again outperforms TCE(SM) under substantially larger mismatch.

**Adroit Tasks.** Adroit tasks present higher-dimensional state spaces and more complex contact-rich dynamics than locomotion tasks, leading to substantially larger domain gaps. We therefore focus on TCE(OG), which is better suited to regimes where direct source mixing is unreliable. As shown in Table 2, TCE(OG) achieves the best performance across all tasks, outperforming all baselines. These results demonstrate that target-aligned generation remains effective even in high-dimensional manipulation settings, and highlight its robustness under severe distributional mismatch.

Table 2: Performance comparison on Adroit tasks from the ODRL benchmark.

Env	Shift	Level	IQL*	DARA	BOSA	IGDF	OTDF	MOBODY	TCE(OG)
Pen	broken-joint	M	15.5 ± 3.4	33.8 ± 2.8	20.4 ± 2.5	29.8 ± 2.8	36.6 ± 2.9	41.3 ± 3.5	<b>59.6 ± 3.7</b>
		H	24.1 ± 1.6	13.3 ± 3.3	19.8 ± 1.3	14.0 ± 1.9	40.1 ± 4.1	34.5 ± 3.1	<b>44.8 ± 2.2</b>
	shrink-finger	M	18.6 ± 2.2	16.2 ± 3.3	17.4 ± 1.3	22.2 ± 0.9	<u>34.5 ± 5.0</u>	24.9 ± 2.0	<b>38.6 ± 3.1</b>
		H	16.4 ± 1.7	24.5 ± 2.8	9.5 ± 1.6	23.5 ± 7.2	<u>32.4 ± 3.9</u>	29.7 ± 1.5	<b>51.9 ± 4.2</b>
Door	broken-joint	M	50.8 ± 2.4	50.9 ± 6.2	47.8 ± 5.4	73.2 ± 8.8	80.4 ± 1.6	79.4 ± 1.8	<b>82.8 ± 1.3</b>
		H	50.7 ± 7.2	36.2 ± 4.5	8.8 ± 2.1	53.4 ± 7.6	<u>78.5 ± 2.1</u>	54.3 ± 2.3	<b>91.8 ± 0.9</b>
	shrink-finger	M	28.3 ± 5.2	58.6 ± 8.4	0.8 ± 0.2	73.2 ± 9.1	<u>70.2 ± 1.1</u>	50.6 ± 0.9	<b>77.2 ± 3.0</b>
		H	14.1 ± 7.7	8.8 ± 1.9	9.3 ± 1.0	35.0 ± 6.5	<u>56.5 ± 2.0</u>	42.6 ± 2.4	<b>57.2 ± 5.7</b>
Total Score			218.5	242.3	143.8	324.3	<u>428.8</u>	357.3	<b>504.0</b>

### 5.3 Analysis of Sample Reliability under Coverage Expansion

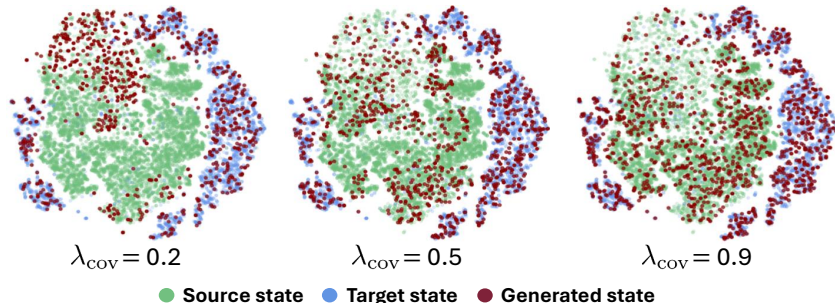


Figure 4: Coverage analysis under varying  $\lambda_{\text{cov}}$ : t-SNE visualization for Ant morphology shifts.

Table 3: Error analysis across coverage settings on MuJoCo morphology shifts (averaged over 36 tasks), reporting action, reward, and transition errors together with normalized score.

Model	$\lambda_{\text{cov}}$	Prediction error			Normalized score
		Action	Reward	Transition	
TCE(OG)	0 (Simple Aug.)	<b>0.038 ± 0.009</b>	<b>0.024 ± 0.010</b>	<b>0.016 ± 0.005</b>	54.6 ± 25.1
	0.1	0.062 ± 0.011	0.025 ± 0.012	0.024 ± 0.013	55.8 ± 24.1
	0.2 (Default)	0.066 ± 0.014	0.025 ± 0.013	0.029 ± 0.012	<b>57.4 ± 24.6</b>
	0.5	0.085 ± 0.021	0.052 ± 0.014	0.046 ± 0.015	52.1 ± 25.5
	0.9	0.118 ± 0.020	0.069 ± 0.017	0.052 ± 0.019	50.9 ± 26.1
TCE (one-stage)	0.2	–	0.105 ± 0.015	0.159 ± 0.052	46.5 ± 22.6

To analyze how coverage expansion affects generation error and performance, we present Fig. 4 and Table 3. Fig. 4 shows that increasing  $\lambda_{\text{cov}}$  expands the covered state region, enabling the model to learn target-aligned behavior on previously unseen states and improving performance initially; however, as coverage further expands, the generation error  $D_{\text{TV}}(\hat{P}_{\text{tar}} \| P_{\text{tar}})$  increases and eventually degrades performance. Table 3 quantifies **this coverage–error trade-off** through action, reward, and transition errors together with normalized score, and compares our two-stage design with **TCE (one-stage)**, which directly estimates  $\hat{P}_{\text{tar}}(s' | s, a)$ .

As in Fig. 2,  $\lambda_{\text{cov}} = 0$  corresponds to Simple Augmentation (Simple Aug.), whose strong performance suggests the benefit of self-augmentation and justifies incorporating target states into the mixture-state distribution. As  $\lambda_{\text{cov}}$  increases, broader coverage improves performance up to a point, after which the error term  $D_{\text{TV}}(\hat{P}_{\text{tar}} \| P_{\text{tar}})$  grows, as predicted by Theorem 4.1, leading to degradation. In Table 3,  $\lambda_{\text{cov}} = 0.2$  achieves the best average score across environments, motivating our default choice.

The same table further highlights the importance of the two-stage design. At  $\lambda_{\text{cov}} = 0.2$ , the target dataset contains only about 5K transitions, making direct estimation of  $s'$  from  $(s, a)$  prone to overfitting. As a result, TCE (one-stage) yields substantially larger reward and transition errors and a much lower normalized score, with errors even exceeding those at  $\lambda_{\text{cov}} = 0.9$ . Overall, these results show that (i) performance is governed by a coverage–error trade-off, (ii) controlling  $\lambda_{\text{cov}}$  is essential, and (iii) the two-stage design is critical for maintaining low generation error under limited target data. Appendix E further visualizes how sample errors increase with  $\lambda_{\text{cov}}$  across MuJoCo environments.

Setting	Avg. Score
TCE(OG)	<b>57.4±24.6</b>
TCE(SM)	48.1±25.5
TCE(OT)	55.6±24.2
TCE(OG) w/o Reg.	55.8±26.8
IQL*	31.5±21.2

(a) Component evaluation

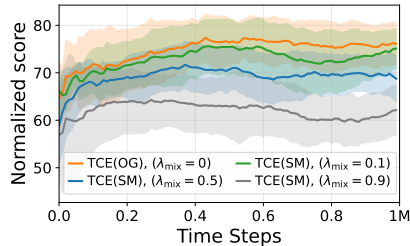
(b) Mixture coefficient  $\lambda_{\text{mix}}$ 

Figure 5: Additional ablation study: (a) component evaluation under morphology shifts (averaged over 36 tasks). (b) effect of the mixture coefficient  $\lambda_{\text{mix}}$  under Ant morphology shifts.

## 5.4 Further Ablation and Analysis

We next present additional ablation results and more in-depth analyses of TCE.

**Component Evaluation.** Fig. 5(a) reports average returns under morphology shifts for TCE(OG), TCE(OT), which replaces the NN criterion with the optimal-transport distance of Lyu et al. [15], and TCE(OG) w/o Reg., which removes the policy regularization term. TCE(OG) performs best overall, indicating that each component contributes to performance. TCE(OT) improves upon TCE(SM) but remains slightly below TCE(OG), suggesting that the selection metric is less critical than controlling the two domain gaps. Removing regularization leads to a modest drop, confirming that the policy regularization term provides additional benefit.

**Mixture Coefficient  $\lambda_{\text{mix}}$ .** In TCE,  $\lambda_{\text{mix}}$  controls how much target-near source data is incorporated into policy learning. Fig. 5(b) fixes  $\lambda_{\text{cov}} = 0.2$  and varies  $\lambda_{\text{mix}}$ . For Ant morphology shifts, where the domain gap is large, TCE(OG) with  $\lambda_{\text{mix}} = 0$  performs best, while TCE(SM) degrades as  $\lambda_{\text{mix}}$  increases, indicating that TCE(OG) is a sensible default in large-gap regimes. In contrast, Appendix G shows that under smaller domain gaps, such as gravity shifts, TCE(SM) can outperform TCE(OG), making the choice of  $\lambda_{\text{mix}}$  beneficial in these settings.

**Further Analysis.** Appendix F provides a computational complexity comparison, showing that TCE incurs only moderate additional training time relative to the baselines while maintaining comparable GPU memory usage, indicating that the overhead is justified by the performance gains. Appendix G.1 shows that wider search ranges for  $\lambda_{\text{mix}}$  and  $\lambda_{\text{cov}}$  yield trends consistent with the main results, suggesting that the practical tuning range is narrow. Appendix G.2 demonstrates that varying the target-data size affects inverse-dynamics error and policy performance in a consistent manner, while TCE remains effective even in the scarce-data regime. Appendix G.3 shows that the denoising step  $K$  has limited impact on performance, indicating that TCE is not sensitive to this choice.

## 6 Limitations and Future Work

Although TCE consistently outperforms baselines, it has several limitations. TCE incurs additional training cost for the score networks and introduces hyperparameters for coverage expansion and data mixing. However, the sampling cost and GPU usage remain comparable to the baselines, and the added training overhead is moderate given the performance gains. Moreover, our experiments suggest that the practical search range of the hyperparameters is narrow and easy to tune. In addition, while TCE is effective under large domain gaps, it does not yet extend to extremely mismatched settings where the source and target share little support, including cases with different state or action spaces. Extending the framework to such settings remains an important direction for future work.

## 7 Conclusion

We presented TCE, a framework that controls the performance gap induced by source data based on our theoretical analysis, balancing target-near source mixing and generation-based coverage expansion. TCE generates target-aligned transitions via a two-stage score-based model to expand target state coverage, mitigating distributional mismatch in cross-domain offline RL and enabling effective policy learning with limited target data. Experiments across diverse MuJoCo domain shifts show that TCE consistently outperforms prior methods, highlighting it as a simple and practical solution for cross-domain offline RL.

## References

- [1] Omer Gottesman, Fredrik D. Johansson, Joshua Meier, Jack Dent, Donghun Lee, Srivatsan Srinivasan, Linying Zhang, Yi Ding, David Wihl, Xuefeng Peng, Jiayu Yao, Isaac Lage, Christopher Mosch, Li-Wei H. Lehman, Matthieu Komorowski, Aldo Faisal, Leo Anthony Celi, David A. Sontag, and Finale Doshi-Velez. Evaluating reinforcement learning algorithms in observational health settings. CoRR, abs/1805.12298, 2018.
- [2] Ekim Yurtsever, Jacob Lambert, Alexander Carballo, and Kazuya Takeda. A survey of autonomous driving: Common practices and emerging technologies. IEEE access, 8:58443–58469, 2020.
- [3] Benjamin Eysenbach, Swapnil Asawa, Shreyas Chaudhari, Ruslan Salakhutdinov, and Sergey Levine. Off-dynamics reinforcement learning: Training for transfer with domain classifiers. In 4th Lifelong Machine Learning Workshop at ICML 2020, 2020.
- [4] Kuno Kim, Yihong Gu, Jiaming Song, Shengjia Zhao, and Stefano Ermon. Domain adaptive imitation learning. In International Conference on Machine Learning, pages 5286–5295. PMLR, 2020.
- [5] Sergey Levine, Aviral Kumar, George Tucker, and Justin Fu. Offline reinforcement learning: Tutorial, review, and perspectives on open problems. CoRR, abs/2005.01643, 2020.
- [6] Jinxin Liu, Zhang Hongyin, and Donglin Wang. DARA: Dynamics-aware reward augmentation in offline reinforcement learning. In International Conference on Learning Representations, 2022.
- [7] Ben Poole, Sherjil Ozair, Aäron van den Oord, Alexander A. Alemi, and George Tucker. On variational bounds of mutual information. In ICML, volume 97 of Proceedings of Machine Learning Research, pages 5171–5180. PMLR, 2019.
- [8] Qing Guo, Junya Chen, Dong Wang, Yuewei Yang, Xinwei Deng, Jing Huang, Larry Carin, Fan Li, and Chenyang Tao. Tight mutual information estimation with contrastive fenchel-legendre optimization. Advances in Neural Information Processing Systems, 35:28319–28334, 2022.
- [9] Kang Xu, Chenjia Bai, Xiaoteng Ma, Dong Wang, Bin Zhao, Zhen Wang, Xuelong Li, and Wei Li. Cross-domain policy adaptation via value-guided data filtering. In Thirty-seventh Conference on Neural Information Processing Systems, 2023.
- [10] Jiafei Lyu, Chenjia Bai, Jingwen Yang, Zongqing Lu, and Xiu Li. Cross-domain policy adaptation by capturing representation mismatch. arXiv preprint arXiv:2405.15369, 2024.
- [11] Aviral Kumar, Aurick Zhou, George Tucker, and Sergey Levine. Conservative q-learning for offline reinforcement learning. Advances in Neural Information Processing Systems, 33: 1179–1191, 2020.
- [12] Ilya Kostrikov, Ashvin Nair, and Sergey Levine. Offline reinforcement learning with implicit q-learning. In International Conference on Learning Representations, 2022.
- [13] Yifan Wu, George Tucker, and Ofir Nachum. Behavior regularized offline reinforcement learning. CoRR, abs/1911.11361, 2019.
- [14] Xiaoyu Wen, Chenjia Bai, Kang Xu, Xudong Yu, Yang Zhang, Xuelong Li, and Zhen Wang. Contrastive representation for data filtering in cross-domain offline reinforcement learning. arXiv preprint arXiv:2405.06192, 2024.
- [15] Jiafei Lyu, Mengbei Yan, Zhongjian Qiao, Runze Liu, Xiaoteng Ma, Deheng Ye, Jing-Wen Yang, Zongqing Lu, and Xiu Li. Cross-domain offline policy adaptation with optimal transport and dataset constraint. In The Thirteenth International Conference on Learning Representations, 2025.
- [16] Tianhe Yu, Aviral Kumar, Yevgen Chebotar, Karol Hausman, Sergey Levine, and Chelsea Finn. Conservative data sharing for multi-task offline reinforcement learning. Advances in Neural Information Processing Systems, 34:11501–11516, 2021.

- [17] Arnaud Fickinger, Samuel Cohen, Stuart Russell, and Brandon Amos. Cross-domain imitation learning via optimal transport. In International Conference on Learning Representations, 2022.
- [18] Sungho Choi, Seungyul Han, Woojun Kim, Jongseong Chae, Whiyoung Jung, and Youngchul Sung. Domain adaptive imitation learning with visual observation. Advances in Neural Information Processing Systems, 36:44067–44104, 2023.
- [19] Jongseong Chae, Seungyul Han, Whiyoung Jung, Myungsik Cho, Sungho Choi, and Youngchul Sung. Robust imitation learning against variations in environment dynamics. In International Conference on Machine Learning, pages 2828–2852. PMLR, 2022.
- [20] Haiyuan Gui, Shanchen Pang, Shihang Yu, Sibao Qiao, Yufeng Qi, Xiao He, Min Wang, and Xue Zhai. Cross-domain policy adaptation with dynamics alignment. Neural Networks, 167: 104–117, 2023.
- [21] Haoyi Niu, Qimao Chen, Tenglong Liu, Jianxiong Li, Guyue Zhou, Yi ZHANG, Jianming HU, and Xianyuan Zhan. xted: Cross-domain adaptation via diffusion-based trajectory editing. In NeurIPS 2024 Workshop on Open-World Agents, 2024.
- [22] Linh Le Pham Van, Minh Hoang Nguyen, Duc Kieu, Hung Le, Sunil Gupta, et al. Dmc: Nearest neighbor guidance diffusion model for offline cross-domain reinforcement learning. In ECAI 2025, pages 2331–2338. IOS Press, 2025.
- [23] Zhongjian Qiao, Rui Yang, Jiafei Lyu, Xiu Li, Zhongxiang Dai, Zhuoran Yang, Siyang Gao, and Shuang Qiu. Dual-robust cross-domain offline reinforcement learning against dynamics shifts. arXiv preprint arXiv:2512.02486, 2025.
- [24] Yihong Guo, Yu Yang, Pan Xu, and Anqi Liu. MOBODY: Model-based off-dynamics offline reinforcement learning. In The Fourteenth International Conference on Learning Representations, 2026. URL <https://openreview.net/forum?id=7c0YS3cuno>.
- [25] Justin Fu, Aviral Kumar, Ofir Nachum, George Tucker, and Sergey Levine. D4RL: datasets for deep data-driven reinforcement learning. CoRR, abs/2004.07219, 2020.
- [26] Jinxin Liu, Ziqi Zhang, Zhenyu Wei, Zifeng Zhuang, Yachen Kang, Sibao Gai, and Donglin Wang. Beyond OOD state actions: Supported cross-domain offline reinforcement learning. the AAAI Conference on Artificial Intelligence, 2024.
- [27] Guanghe Li, Yixiang Shan, Zhengbang Zhu, Ting Long, and Weinan Zhang. Diffstitch: Boosting offline reinforcement learning with diffusion-based trajectory stitching. arXiv preprint arXiv:2402.02439, 2024.
- [28] Yunhao Luo, Utkarsh A Mishra, Yilun Du, and Danfei Xu. Generative trajectory stitching through diffusion composition. arXiv preprint arXiv:2503.05153, 2025.
- [29] Zhi Wang, Li Zhang, Wenhao Wu, Yuanheng Zhu, Dongbin Zhao, and Chunlin Chen. Meta-dt: Offline meta-rl as conditional sequence modeling with world model disentanglement. Advances in Neural Information Processing Systems, 37:44845–44870, 2024.
- [30] Yang Song and Stefano Ermon. Generative modeling by estimating gradients of the data distribution. Advances in neural information processing systems, 32, 2019.
- [31] Yang Song and Stefano Ermon. Improved techniques for training score-based generative models. Advances in neural information processing systems, 33:12438–12448, 2020.
- [32] Jonathan Ho, Ajay Jain, and Pieter Abbeel. Denoising diffusion probabilistic models. Advances in neural information processing systems, 33:6840–6851, 2020.
- [33] Alexander Quinn Nichol and Prafulla Dhariwal. Improved denoising diffusion probabilistic models. In International conference on machine learning, pages 8162–8171. PMLR, 2021.
- [34] Prafulla Dhariwal and Alexander Nichol. Diffusion models beat gans on image synthesis. Advances in neural information processing systems, 34:8780–8794, 2021.

- [35] Yang Song, Jascha Sohl-Dickstein, Diederik P Kingma, Abhishek Kumar, Stefano Ermon, and Ben Poole. Score-based generative modeling through stochastic differential equations. arXiv preprint arXiv:2011.13456, 2020.
- [36] Tero Karras, Miika Aittala, Timo Aila, and Samuli Laine. Elucidating the design space of diffusion-based generative models. Advances in neural information processing systems, 35: 26565–26577, 2022.
- [37] Ian J Goodfellow, Jean Pouget-Abadie, Mehdi Mirza, Bing Xu, David Warde-Farley, Sherjil Ozair, Aaron Courville, and Yoshua Bengio. Generative adversarial nets. Advances in neural information processing systems, 27, 2014.
- [38] Diederik P Kingma and Max Welling. Auto-encoding variational bayes. arXiv preprint arXiv:1312.6114, 2013.
- [39] Emanuel Todorov, Tom Erez, and Yuval Tassa. Mujoco: A physics engine for model-based control. In 2012 IEEE/RSJ international conference on intelligent robots and systems, pages 5026–5033. IEEE, 2012.
- [40] Jiafei Lyu, Kang Xu, Jiacheng Xu, Jing-Wen Yang, Zongzhang Zhang, Chenjia Bai, Zongqing Lu, Xiu Li, et al. Odr1: A benchmark for off-dynamics reinforcement learning. Advances in Neural Information Processing Systems, 37:59859–59911, 2024.
- [41] Zhenghai Xue, Qingpeng Cai, Shuchang Liu, Dong Zheng, Peng Jiang, Kun Gai, and Bo An. State regularized policy optimization on data with dynamics shift. In Thirty-seventh Conference on Neural Information Processing Systems, 2023.

## A Proof of Theorem 4.1

We begin by introducing the *Telescoping Lemma* [9], a fundamental result that decomposes the performance difference between two MDPs arising from their dynamic mismatch. This lemma serves as a cornerstone for our analysis.

**Lemma A.1** (Telescoping Lemma, Lemma C.1 in Xu et al. [9]). *Let  $\mathcal{M}_1 := (\mathcal{S}, \mathcal{A}, P_1, r, \gamma)$  and  $\mathcal{M}_2 := (\mathcal{S}, \mathcal{A}, P_2, r, \gamma)$  be two MDPs differing only in their transition dynamics  $P_1$  and  $P_2$ . For any policy  $\pi$ , defining the value discrepancy term as*

$$G_{\mathcal{M}_1, \mathcal{M}_2}^\pi(s, a) := \mathbb{E}_{s' \sim P_1} [V_{\mathcal{M}_2}^\pi(s')] - \mathbb{E}_{s' \sim P_2} [V_{\mathcal{M}_2}^\pi(s')],$$

allows us to express the performance gap as:

$$\eta_{\mathcal{M}_1}(\pi) - \eta_{\mathcal{M}_2}(\pi) = \frac{\gamma}{1 - \gamma} \mathbb{E}_{(s,a) \sim \rho_{\mathcal{M}_1}^\pi} [G_{\mathcal{M}_1, \mathcal{M}_2}^\pi(s, a)].$$

The proof of Lemma A.1 is provided in Xu et al. [9]. Building upon this result, we restate and prove our main theorem, which bounds the performance gap between the mixture and target domains from the perspective of transition dynamics.

**Theorem 4.1** (Performance Gap via Total Variation). *Let  $\eta_{\text{mix}}(\pi)$  and  $\rho_{\text{mix}}^\pi$  denote the expected return and the state-action occupancy measure in the mixture MDP, respectively. Then, the performance gap between the target MDP and the mixture MDP can be bounded in terms of transition dynamics as follows:*

$$\eta_{\text{mix}}(\pi) - \eta_{\text{tar}}(\pi) \leq \frac{2\gamma r_{\max}}{(1 - \gamma)^2} \left( \lambda \mathbb{E}_{\rho_{\text{mix}}^\pi} [D_{\text{TV}}(P_{\text{src}} \| P_{\text{tar}})] + (1 - \lambda) \mathbb{E}_{\rho_{\text{mix}}^\pi} [D_{\text{TV}}(\hat{P}_{\text{tar}} \| P_{\text{tar}})] \right), \quad (9)$$

where  $r_{\max}$  denotes the maximum reward and  $D_{\text{TV}}(P \| Q)$  denotes the total variation distance between  $P$  and  $Q$ .

*Proof.* To simplify notation, let  $P_{\text{mix}}$ ,  $P_{\text{src}}$ , and  $P_{\text{tar}}$  denote  $P_{\text{mix}}(\cdot | s, a)$ ,  $P_{\text{src}}(\cdot | s, a)$ , and  $P_{\text{tar}}(\cdot | s, a)$  respectively. Similarly,  $\rho_{\text{mix}}^\pi$  denotes  $\rho_{\text{mix}}^\pi(s, a)$ , and  $V_{\text{tar}}^\pi$  represents  $V_{\text{tar}}^\pi(s')$ .

Applying Lemma A.1 with  $\mathcal{M}_1 = \text{mix}$  and  $\mathcal{M}_2 = \text{tar}$ , we have:

$$\begin{aligned} \eta_{\text{mix}}(\pi) - \eta_{\text{tar}}(\pi) &= \frac{\gamma}{1 - \gamma} \mathbb{E}_{\rho_{\text{mix}}^\pi} \left[ \int P_{\text{mix}} V_{\text{tar}}^\pi ds' - \int P_{\text{tar}} V_{\text{tar}}^\pi ds' \right] && \text{(by Lemma A.1)} \\ &= \frac{\gamma}{1 - \gamma} \mathbb{E}_{\rho_{\text{mix}}^\pi} \left[ \int (P_{\text{mix}} - P_{\text{tar}}) V_{\text{tar}}^\pi ds' \right] \\ &\leq \frac{\gamma}{1 - \gamma} \mathbb{E}_{\rho_{\text{mix}}^\pi} \left[ \int |P_{\text{mix}} - P_{\text{tar}}| \cdot |V_{\text{tar}}^\pi| ds' \right] && \text{(Triangle Inequality)} \\ &\leq \frac{\gamma}{1 - \gamma} \cdot \frac{r_{\max}}{1 - \gamma} \mathbb{E}_{\rho_{\text{mix}}^\pi} \left[ \int |P_{\text{mix}} - P_{\text{tar}}| ds' \right] \\ &= \frac{2\gamma r_{\max}}{(1 - \gamma)^2} \mathbb{E}_{\rho_{\text{mix}}^\pi} \left[ \frac{1}{2} \int |P_{\text{mix}} - P_{\text{tar}}| ds' \right] \\ &= \frac{2\gamma r_{\max}}{(1 - \gamma)^2} \mathbb{E}_{\rho_{\text{mix}}^\pi} [D_{\text{TV}}(P_{\text{mix}} \| P_{\text{tar}})] \\ &= \frac{2\gamma r_{\max}}{(1 - \gamma)^2} \mathbb{E}_{\rho_{\text{mix}}^\pi} [D_{\text{TV}}((\lambda P_{\text{src}} + (1 - \lambda) \hat{P}_{\text{tar}}) \| P_{\text{tar}})] \\ &\leq \frac{2\gamma r_{\max}}{(1 - \gamma)^2} \mathbb{E}_{\rho_{\text{mix}}^\pi} [\lambda D_{\text{TV}}(P_{\text{src}} \| P_{\text{tar}}) + (1 - \lambda) D_{\text{TV}}(\hat{P}_{\text{tar}} \| P_{\text{tar}})] \end{aligned}$$

where the inequality follows from the convexity of total variation distance, yielding the desired bound.  $\square$

While Theorem 4.1 bounds the performance gap using the total variation distance between transition dynamics, it is also insightful to analyze this gap from the perspective of value discrepancy. This alternative view highlights how errors in value estimation under different dynamics contribute to the overall performance difference.

**Theorem 4.2** (Performance Gap via Value Discrepancy). *Under the same assumptions as Theorem 4.1, the performance gap between the mixture MDP and the target MDP satisfies:*

$$\begin{aligned} \eta_{\text{mix}}(\pi) - \eta_{\text{tar}}(\pi) &\leq \frac{\gamma}{1-\gamma} \left( \lambda \mathbb{E}_{\rho_{\text{mix}}^{\pi}} \left[ \left| \mathbb{E}_{P_{\text{src}}} [V_{\text{tar}}^{\pi}(s')] - \mathbb{E}_{P_{\text{tar}}} [V_{\text{tar}}^{\pi}(s')] \right| \right] \right. \\ &\quad \left. + (1-\lambda) \mathbb{E}_{\rho_{\text{mix}}^{\pi}} \left[ \left| \mathbb{E}_{\hat{P}_{\text{tar}}} [V_{\text{tar}}^{\pi}(s')] - \mathbb{E}_{P_{\text{tar}}} [V_{\text{tar}}^{\pi}(s')] \right| \right] \right). \end{aligned} \quad (10)$$

*Proof.* To simplify notation, let  $P_{\text{mix}}$ ,  $P_{\text{src}}$ , and  $P_{\text{tar}}$  denote  $P_{\text{mix}}(\cdot | s, a)$ ,  $P_{\text{src}}(\cdot | s, a)$ , and  $P_{\text{tar}}(\cdot | s, a)$  respectively. Similarly,  $\rho_{\text{mix}}^{\pi}$  denotes  $\rho_{\text{mix}}^{\pi}(s, a)$ , and  $V_{\text{tar}}^{\pi}$  represents  $V_{\text{tar}}^{\pi}(s')$ .

Applying Lemma A.1 with  $\mathcal{M}_1 = \text{mix}$  and  $\mathcal{M}_2 = \text{tar}$ , we have:

$$\begin{aligned} \eta_{\text{mix}}(\pi) - \eta_{\text{tar}}(\pi) &= \frac{\gamma}{1-\gamma} \mathbb{E}_{\rho_{\text{mix}}^{\pi}} \left[ \int P_{\text{mix}} V_{\text{tar}}^{\pi} ds' - \int P_{\text{tar}} V_{\text{tar}}^{\pi} ds' \right] \quad (\text{by Lemma A.1}) \\ &= \frac{\gamma}{1-\gamma} \mathbb{E}_{\rho_{\text{mix}}^{\pi}} \left[ \mathbb{E}_{P_{\text{mix}}} [V_{\text{tar}}^{\pi}(s')] - \mathbb{E}_{P_{\text{tar}}} [V_{\text{tar}}^{\pi}(s')] \right] \\ &\leq \frac{\gamma}{1-\gamma} \mathbb{E}_{\rho_{\text{mix}}^{\pi}} \left[ \left| \mathbb{E}_{P_{\text{mix}}} [V_{\text{tar}}^{\pi}(s')] - \mathbb{E}_{P_{\text{tar}}} [V_{\text{tar}}^{\pi}(s')] \right| \right] \\ &= \frac{\gamma}{1-\gamma} \mathbb{E}_{\rho_{\text{mix}}^{\pi}} \left[ \left| \lambda \mathbb{E}_{P_{\text{src}}} [V_{\text{tar}}^{\pi}(s')] + (1-\lambda) \mathbb{E}_{\hat{P}_{\text{tar}}} [V_{\text{tar}}^{\pi}(s')] - \mathbb{E}_{P_{\text{tar}}} [V_{\text{tar}}^{\pi}(s')] \right| \right] \\ &= \frac{\gamma}{1-\gamma} \mathbb{E}_{\rho_{\text{mix}}^{\pi}} \left[ \left| \lambda (\mathbb{E}_{P_{\text{src}}} [V_{\text{tar}}^{\pi}(s')] - \mathbb{E}_{P_{\text{tar}}} [V_{\text{tar}}^{\pi}(s')]) \right. \right. \\ &\quad \left. \left. + (1-\lambda) (\mathbb{E}_{\hat{P}_{\text{tar}}} [V_{\text{tar}}^{\pi}(s')] - \mathbb{E}_{P_{\text{tar}}} [V_{\text{tar}}^{\pi}(s')]) \right| \right] \\ &\leq \frac{\gamma}{1-\gamma} \mathbb{E}_{\rho_{\text{mix}}^{\pi}} \left[ \left| \lambda \left| \mathbb{E}_{P_{\text{src}}} [V_{\text{tar}}^{\pi}(s')] - \mathbb{E}_{P_{\text{tar}}} [V_{\text{tar}}^{\pi}(s')] \right| \right. \right. \\ &\quad \left. \left. + (1-\lambda) \left| \mathbb{E}_{\hat{P}_{\text{tar}}} [V_{\text{tar}}^{\pi}(s')] - \mathbb{E}_{P_{\text{tar}}} [V_{\text{tar}}^{\pi}(s')] \right| \right| \right] \end{aligned}$$

where the last inequality follows from the triangle inequality, proving the claim.  $\square$

The derived bounds (Theorem 4.1 and Theorem 4.2) consistently highlight two distinct avenues for reducing the performance discrepancy. Whether viewed through transition dynamics or value estimates, the gap is governed by the alignment between source and target dynamics and the accuracy of the generative model. Coefficient  $\lambda$  explicitly controls the trade-off between these two sources of error, enabling us to attenuate the influence of irreducible source-target mismatches while leveraging accurate target-like generations to tighten the overall performance bound.

## B Detailed Implementation and Algorithm of TCE

This section summarizes core components of our proposed TCE method: Subsection B.1 provides the configuration of the score-based generative models. Subsection B.2 details the auxiliary models, dataset construction, and the offline policy learning. Subsection B.3 provides network architecture and configuration details supporting the overall implementation.

### B.1 Details of Score-based Generative Model with SDEs

Our generative framework follows the score-based modeling with SDEs described in Section 3.2. We adopt the variance exploding (VE) SDE formulation with drift  $f(x, \tau) = 0$  and diffusion coefficient  $g(\tau) = \sqrt{d(\sigma^2)/d\tau}$ . In our implementation, we use a VP-style variance schedule while retaining the VE reverse-time dynamics and predictor-corrector sampling, which can be viewed as a parameterization choice within the score-SDE framework. The noise scale  $\sigma(\tau)$  is defined using a quadratic schedule for the exponent  $\mathcal{B}(\tau)$ :

$$\sigma(\tau) = \sqrt{1 - \exp(-\mathcal{B}(\tau))}, \quad \mathcal{B}(\tau) = \alpha_{\min}\tau + \frac{1}{2}(\alpha_{\max} - \alpha_{\min})\tau^2, \quad (11)$$

where we fix  $\alpha_{\min} = 0.1$  and  $\alpha_{\max} = 20$  to ensure a smooth noise injection process. This choice is better suited to our low-dimensional, data-scarce offline RL setting than the canonical geometric VE schedule, as it gives smoother noise growth and more stable score estimation under limited data.

The score network is optimized via the denoising score matching loss (Eq. (1) in main text) using the weighting function  $\zeta(\tau) = \sigma(\tau)^2$ . In the absence of conditional input  $c$ , this formulation simplifies to an unconditional score network  $q_\theta(x^\tau, \tau)$ .

For sample generation, we employ the predictor-corrector (PC) scheme with  $K = 500$  discretization steps. This method combines a numerical SDE solver (Predictor) with Langevin dynamics (Corrector) to improve robustness and sample quality. Specifically, at each timestep, the predictor integrates the reverse SDE:

$$\text{(Predictor)} \quad x^{k-1} = x^k - g(\tau^k)^2 q_\theta(x^k, \tau^k | c) \Delta\tau^k + g(\tau^k) \sqrt{|\Delta\tau^k|} \xi^k, \quad \xi^k \sim \mathcal{N}(0, I). \quad (12)$$

Following the predictor step, a Langevin corrector step refines the sample based on the score function:

$$\text{(Corrector)} \quad x^{k-1} \leftarrow x^{k-1} + \eta^k q_\theta(x^{k-1}, \tau^{k-1} | c) + \sqrt{2\eta^k} \xi^k, \quad \xi^k \sim \mathcal{N}(0, I), \quad (13)$$

where  $\eta^k$  is a step-size parameter for the corrector. This refinement helps correct errors accumulated during the numerical integration, yielding higher-quality transitions.

### B.2 Detailed Implementation of TCE

In this section, we provide implementation details for the auxiliary models, the dataset construction, and the offline policy learning. The training and sampling for the score-based generative models follow the methodology described in Section 4.3.

**Auxiliary Models and Labeling.** Since the score-based models generate only state transitions  $(\hat{s}_t, \hat{s}_{t+1})$ , we require auxiliary models to recover the missing actions and rewards. We train an inverse dynamics model  $\text{Inv}_\psi$  and a reward model  $R_\psi$  using the mean squared error (MSE) loss:

$$\mathcal{L}_{\text{aux}}(\psi) = \underbrace{\mathbb{E}_{\mathcal{D}_{\text{tar}}} \|\text{Inv}_\psi(s_t, s_{t+1}) - a_t\|_2^2}_{\text{Inverse dynamics loss}} + \underbrace{\mathbb{E}_{\mathcal{D}_{\text{tar}} \cup \mathcal{D}_{\text{src}}^{\lambda_{\text{cov}}}} \|R_\psi(s_t, a_t, s_{t+1}) - r_t\|_2^2}_{\text{Reward loss}}. \quad (14)$$

The inverse dynamics model is trained solely on  $\mathcal{D}_{\text{tar}}$  to ensure consistency with target dynamics, while the reward model is trained on  $\mathcal{D}_{\text{tar}} \cup \mathcal{D}_{\text{src}}^{\lambda_{\text{cov}}}$  to leverage the shared reward function. We then utilize these models to label the generated state transitions  $(\hat{s}_t, \hat{s}_{t+1})$  with actions and rewards, forming the fully labeled dataset  $\mathcal{D}_{\text{gen}}^{\lambda_{\text{cov}}}$ . This labeled dataset is combined with the original data to form the final training set.

**Dataset Construction and IQL Training.** We construct the final training dataset  $\mathcal{D}_{\text{train}}$  by augmenting  $\mathcal{D}_{\text{tar}}$  with generated and source transitions. To maintain a consistent data volume, we set  $|\mathcal{D}_{\text{gen}}^{\lambda_{\text{cov}}}| = (1 - \lambda_{\text{mix}})|\mathcal{D}_{\text{src}}|$ . Based on the mixture coefficient  $\lambda_{\text{mix}}$ , we define **TCE(OG)** ( $\lambda_{\text{mix}} = 0$ ) as  $\mathcal{D}_{\text{train}} := \mathcal{D}_{\text{tar}} \cup \mathcal{D}_{\text{gen}}^{\lambda_{\text{cov}}}$ , and **TCE(SM)** ( $\lambda_{\text{mix}} > 0$ ) as  $\mathcal{D}_{\text{train}} := \mathcal{D}_{\text{tar}} \cup \mathcal{D}_{\text{src}}^{\lambda_{\text{mix}}} \cup \mathcal{D}_{\text{gen}}^{\lambda_{\text{cov}}}$ .

For policy learning, we employ Implicit Q-Learning (IQL) [12] on  $\mathcal{D}_{\text{train}}$ . The training objectives for the value function  $V_\varphi$ , Q-function  $Q_\varphi$ , and policy  $\pi_\omega$  are defined as follows:

$$\mathcal{L}_V(\varphi) = \mathbb{E}_{(s_t, a_t) \sim \mathcal{D}_{\text{train}}} [L_2^{\tau_V}(Q_{\varphi'}(s_t, a_t) - V_\varphi(s_t))], \quad (15)$$

$$\mathcal{L}_Q(\varphi) = \mathbb{E}_{(s_t, a_t, r_t, s_{t+1}) \sim \mathcal{D}_{\text{train}}} [(r_t + \gamma V_{\varphi^-}(s_{t+1}) - Q_\varphi(s_t, a_t))^2], \quad (16)$$

$$\begin{aligned} \mathcal{L}_\pi(\omega) = & \mathbb{E}_{(s_t, a_t) \sim \mathcal{D}_{\text{train}}} [\exp(\kappa \cdot \text{Adv}(s_t, a_t)) \log \pi_\omega(a_t | s_t)] \\ & + \beta \mathbb{E}_{s_t \sim \mathcal{D}_{\text{tar}}} [D_{\text{KL}}(\hat{\pi}_b(\cdot | s_t) \| \pi_\omega(\cdot | s_t))], \end{aligned} \quad (17)$$

where  $L_2^{\tau_V}(u) = |\tau_V - \mathbb{1}[u < 0]| u^2$  is the expectile loss with  $\tau_V = 0.7$ ;  $\varphi'$  and  $\varphi^-$  denote the target network and stop-gradient parameters, respectively;  $\text{Adv}(s_t, a_t) = Q_\varphi(s_t, a_t) - V_\varphi(s_t)$  is the advantage weighted by temperature  $\kappa = 3$ ; and  $\hat{\pi}_b$  is the empirical behavior policy cloned from  $\mathcal{D}_{\text{tar}}$ , with  $\beta$  controlling the KL-divergence penalty.

### B.3 Network Architecture and Configurations

We employ four core neural network architectures to model mixture-state scores, target-transition scores, inverse dynamics, and reward estimation. As summarized in Table 4, all networks leverage MLP backbones with residual connections to ensure effective gradient flow. Details of environment-specific state and action dimensions ( $d_s$  and  $d_a$ ) are provided in Table 5.

**Mixture state score network** ( $q_\theta^{\text{mix}}$ ) estimates the score of perturbed states conditioned on diffusion time. It takes the state  $s_t$  and time  $\tau$  as inputs. The time input is embedded via a 2-layer MLP, concatenated with  $s_t$ , and processed through residual dense blocks before a final projection to  $\mathbb{R}^{d_s}$ .

**Target-transition score network** ( $q_\theta^{\text{tran}}$ ) predicts the score of the next state  $s_{t+1}$  conditioned on  $s_t$  and  $\tau$ . Similar to the state score network, it embeds both  $\tau$  and  $s_t$  using separate MLPs. These embeddings are concatenated with  $s_{t+1}$  and passed through residual blocks to output a score in  $\mathbb{R}^{d_s}$ .

**Inverse dynamics (Inv $_\psi$ ) and Reward models ( $R_\psi$ )** map state transition pairs  $[s_t, s_{t+1}]$  to the action space  $\mathbb{R}^{d_a}$  and scalar rewards, respectively. Both networks share the same architecture, starting with a dense layer followed by residual blocks.

Table 4: Detailed architectures of the score and dynamics models.

**Notation:** MLP( $x; [h_1, \dots, h_k]$ ) denotes an MLP with hidden sizes  $h_i$  and SiLU activations. Linear( $d$ ) is a fully connected layer with output dimension  $d$ . [ResBlock( $d$ )] $_{\times N}$  denotes a stack of  $N$  residual MLP blocks.

Network	Inputs	Architecture Specification
Mixture-state score ( $q_\theta^{\text{mix}}$ )	State $s_t$ Time $\tau$	$h_\tau = \text{MLP}(\tau; [128, 128])$ $h_{\text{in}} = \text{Concat}[s_t, h_\tau]$ $\text{MLP}(h_{\text{in}}; [256]) \rightarrow [\text{ResBlock}(256)]_{\times 4} \rightarrow \text{Linear}(d_s)$
Target-transition score ( $q_\theta^{\text{tran}}$ )	State $s_t$ Time $\tau$ Next state $s_{t+1}$	$h_\tau = \text{MLP}(\tau; [128, 128])$ $h_s = \text{MLP}(s_t; [128, 128])$ $h_{\text{in}} = \text{Concat}[s_{t+1}, h_\tau, h_s]$ $\text{MLP}(h_{\text{in}}; [256]) \rightarrow [\text{ResBlock}(256)]_{\times 4} \rightarrow \text{Linear}(d_s)$
Inverse dynamics model (Inv $_\psi$ )	State $s_t$ Next state $s_{t+1}$	$h_{\text{in}} = \text{Concat}[s_t, s_{t+1}]$ $\text{MLP}(h_{\text{in}}; [256]) \rightarrow [\text{ResBlock}(256)]_{\times 3} \rightarrow \text{Linear}(d_a)$
Reward model ( $R_\psi$ )	State $s_t$ Next state $s_{t+1}$	$h_{\text{in}} = \text{Concat}[s_t, s_{t+1}]$ $\text{MLP}(h_{\text{in}}; [256]) \rightarrow [\text{ResBlock}(256)]_{\times 3} \rightarrow \text{Linear}(1)$

Table 5: State dimension ( $d_s$ ) and action dimension ( $d_a$ ) of each agent.

Agent Type	State Dimension ( $d_s$ )	Action Dimension ( $d_a$ )
HalfCheetah, Walker2d	17	6
Hopper	11	3
Ant	111	8
Pen	45	24
Door	39	24

## C Detailed Experimental Setup

This section outlines the experimental setup in detail. It first summarizes the baselines used for comparison in section C.1, then describes the environment and offline dataset configurations and domain shifts considered in section C.2, and finally presents the hyperparameter choices for model training and algorithm parameters in section C.3.

### C.1 Baselines Explanation

This section summarizes the baseline algorithms used for comparison with TCE approach.

**IQL** [12] is a widely used offline RL method that learns policies strictly within the support of the dataset, avoiding extrapolation to OOD samples. While stable, this design makes it difficult to learn meaningful policies when only limited target-domain data is available. The variant **IQL\*** leverages both source and target datasets to stabilize training and expand state coverage. **Official Code:** [https://github.com/ikostrikov/implicit\\_q\\_learning](https://github.com/ikostrikov/implicit_q_learning).

**DARA** [6] mitigates the effect of dynamics mismatch by training domain classifiers on state-action-next-state and state-action pairs to quantify domain discrepancy. This discrepancy is used to adjust source rewards, encouraging source data to better align with target dynamics. For this method, we follow the implementation provided in [15].

**BOSA** [26] introduces supported value estimation to constrain critic updates to plausible transitions under target dynamics. The actor updates only consider supported actions, preventing exploitation of unsupported out-of-distribution transitions. For this method, we follow the implementation provided in [15].

**SRPO** [41] constrains the learned policy distribution to remain close to the target state distribution by incorporating a KL divergence budget, inducing a reward shaping term via a domain discriminator to enforce consistency with target dynamics. For this method, we follow the implementation provided in [15].

**IGDF** [14] learns cross-domain contrastive representations that distinguish source from target transitions. The resulting scores filter source data during critic training to ensure only reliable source transitions contribute. **Official Code:** <https://github.com/BattleWen/IGDF>.

**OTDF** [15] applies optimal transport to align source and target transitions by computing deviation scores and selectively weighting source samples. The policy update also integrates CVAE-based support regularization to ensure the learned policy remains consistent with the target action. **Official Code:** <https://github.com/dmksjfl/OTDF>.

**MOBODY** [24] is a model-based off-dynamics offline RL method that learns target dynamics from source and limited target data, then performs policy optimization via rollouts from the learned target dynamics. It models source and target with separate action encoders and a shared latent transition, and uses target-Q-weighted behavior cloning for policy regularization. **Official Code:** <https://github.com/guoyihonggyh/MOBODY-Model-Based-Off-Dynamics-Offline-Reinforcement-Learning>.

## C.2 Environmental Setup

This section details the experimental setup used to evaluate our approach. We adopt the cross-domain continuous control setup, including environments, dataset compositions, and domain shift configurations, proposed by Lyu et al. [15]. The benchmark is based on MuJoCo environments [39] and features four agent types: HalfCheetah, Hopper, Walker2d, and Ant. In addition, we evaluate Adroit dexterous-manipulation tasks from the ODRL benchmark [40], which extend the evaluation to higher-dimensional domains with more pronounced structural shifts.

**Offline Datasets.** The offline datasets consist of pre-collected data from both source and target domains, primarily drawn from the D4RL benchmark [25] for MuJoCo tasks and from the ODRL benchmark [40] for Adroit tasks.

**Source domain.** For MuJoCo, source data comprises three quality levels: `medium`, `medium-replay`, and `medium-expert`. The `medium` dataset contains 1M samples generated by a partially trained SAC policy. The `medium-replay` dataset includes all samples in the SAC replay buffer up to the point of medium performance (approx. 0.2M to 0.4M samples), thus mixing low- to medium-quality experiences. Finally, the `medium-expert` datasets combine 50% expert and 50% suboptimal data, with total sizes ranging from 1M to 2M transitions. For Adroit, following ODRL, the source domain consists of expert-demonstration data with roughly 0.5M transitions per task.

**Target domain.** The target domain is used to assess policy adaptation under distributional shifts. For MuJoCo, three types of dynamics changes are introduced to the agents: **Morphology** shift (modifying the agent’s physical structure), **Kinematic** shift (restricting joint rotations to simulate malfunctions), and **Gravity** shift (altering gravitational acceleration). MuJoCo target datasets are limited to a small number of samples (typically under 5K per dataset) and are provided across `medium`, `medium-expert`, and `expert` quality levels. For Adroit, following ODRL, we evaluate two tasks, Pen and Door, under two target-domain shift types: **Morphology** shift (`shrink-finger`, reducing finger capsule sizes) and **Kinematic** shift (`broken-joint`, restricting finger joint ranges). Each target dataset is restricted to 5K transitions. The labels M and H denote medium and hard shift levels. Table 6 summarizes the dataset sizes by domain and quality.

Table 6: Dataset sizes by domain and data quality for MuJoCo and Adroit tasks.

Environment	Source Domain		Target Domain	Morphology	Kinematic	Gravity
HalfCheetah	<code>medium</code>	1M	<code>medium</code>	5K	5K	5K
	<code>medium-replay</code>	0.2M	<code>medium-expert</code>	5K	5K	5K
	<code>medium-expert</code>	2M	<code>expert</code>	5K	5K	5K
Hopper	<code>medium</code>	1M	<code>medium</code>	5K	5K	5K
	<code>medium-replay</code>	0.4M	<code>medium-expert</code>	4.3K	5K	4.3K
	<code>medium-expert</code>	2M	<code>expert</code>	5K	5K	5K
Walker2d	<code>medium</code>	1M	<code>medium</code>	5K	5K	5K
	<code>medium-replay</code>	0.3M	<code>medium-expert</code>	3.5K	4.4K	4.8K
	<code>medium-expert</code>	2M	<code>expert</code>	5K	5K	5K
Ant	<code>medium</code>	1M	<code>medium</code>	5K	5K	5K
	<code>medium-replay</code>	0.3M	<code>medium-expert</code>	5K	5K	3.1K
	<code>medium-expert</code>	2M	<code>expert</code>	5K	5K	5K
Pen	<code>expert</code>	0.5M	<code>expert</code>	5K	5K	–
Door	<code>expert</code>	0.5M	<code>expert</code>	5K	5K	–

**Evaluation Metric.** All results are presented as normalized scores to fairly compare across environments with varying return scales:

$$NS = \frac{J - J_r}{J_e - J_r} \times 100,$$

where  $J$  is the return of the evaluated policy, and  $J_r$  and  $J_e$  represent returns from random and expert policies in the target domain, respectively. Reference scores proposed by Lyu et al. [15] for each agent and target domain scenario are shown in Table 7. For Adroit, the morphology rows below correspond to the shrink-finger shift and the kinematic rows correspond to the broken-joint shift.

Table 7: Reference minimum score  $J_r$  and maximum score  $J_e$  by agent and domain shifts.

Agent Type	Domain Shifts	Reference min score $J_r$	Reference max score $J_e$
HalfCheetah	Morphology	-280.18	9713.59
	Kinematic	-280.18	7065.03
	Gravity	-280.18	9509.15
Hopper	Morphology	-26.34	3152.75
	Kinematic	-26.34	2842.73
	Gravity	-26.34	3234.3
Walker2d	Morphology	10.8	4398.43
	Kinematic	10.8	3257.51
	Gravity	10.8	5154.71
Ant	Morphology	-325.6	5722.01
	Kinematic	-325.6	5122.57
	Gravity	-325.6	4317.07
Pen	Morphology	-12.17	6408.38
	Kinematic	-12.17	6408.38
Door	Morphology	-52.34	2880.57
	Kinematic	-52.34	2880.57

**Domain Shifts.** To simulate realistic but significant distributional differences between source and target domains, we consider separate domain-shift settings for MuJoCo and Adroit. These shifts directly impact the agent’s control dynamics and pose challenges to policy generalization. Fig. 6 provides visual examples of the source domain and the corresponding morphology-shifted target domains, highlighting the structural changes induced by these perturbations.



Figure 6: Visual examples of the source domain and morphology-shifted target domains in MuJoCo.

For MuJoCo tasks, we apply three types of domain shifts:

- *Morphology shift* involves structural modifications to the agent’s body by altering body-segment dimensions. This includes shortening the thighs in HalfCheetah, enlarging the torso in Hopper, elongating the right leg in Walker2d, and reducing the front ankle capsules in Ant. These modifications create clear physical domain gaps that affect locomotion efficiency and balance.

- *Kinematic shift* emulates impairments or restrictions in joint mobility by narrowing the allowed range of joint rotations. This corresponds to restricting the back thigh in HalfCheetah, the head and foot joints in Hopper, the foot joint in Walker2d, and the front hip joints in Ant, thereby reducing maneuverability in the target domain.
- *Gravity shift* reduces the gravitational force magnitude acting on the agents by changing the target-domain gravity from the standard Earth value of  $-9.81 \text{ m/s}^2$  in the source to  $-4.905 \text{ m/s}^2$ . This creates a lighter environment in which the reduced downward force alters the agents' balance, contact dynamics, and overall locomotion efficiency during movement.

For Adroit tasks, following ODRL, we consider two target-domain shift types:

- *Morphology shift* follows the `shrink-finger` setting, which reduces the capsule half-lengths of the finger phalanges, yielding shorter fingers with less contact area for stable grasping.
- *Kinematic shift* follows the `broken-joint` setting, which contracts the rotational ranges of the index-finger and thumb joints, substantially limiting finger dexterity and precise grasp formation.

These domain shifts are implemented by modifying the MuJoCo XML configuration files following Lyu et al. [15] for MuJoCo and the ODRL XML and environment configurations for Adroit. Together, these settings enable a comprehensive evaluation of cross-domain offline reinforcement learning under varied and challenging environment changes.

HalfCheetah morphology shift : thigh length reduced by approximately 99%

```
<geom fromto="0 0 0 -0.0001 0 -0.0001" name="bthigh" size="0.046" type="capsule"/>
<body name="bshin" pos="-0.0001 0 -0.0001">
<geom fromto="0 0 0 0.0001 0 0.0001" name="fthigh" size="0.046" type="capsule"/>
<body name="fshin" pos="0.0001 0 0.0001">
```

Hopper morphology shift : torso length reduced by approximately 56%

```
<geom friction="0.9" fromto="0 0 1.45 0 0 1.05" name="torso_geom" size="0.125" type="capsule
"/>
```

Walker2d morphology shift : thigh shortened and lower leg elongated by approximately 98%

```
<body name="thigh" pos="0 0 1.05">
  <joint axis="0 -1 0" name="thigh_joint" pos="0 0 1.05" range="-150 0" type="hinge"/>
  <geom friction="0.9" fromto="0 0 1.05 0 0 1.045" name="thigh_geom" size="0.05" type="
  capsule"/>
  <body name="leg" pos="0 0 0.35">
    <joint axis="0 -1 0" name="leg_joint" pos="0 0 1.045" range="-150 0" type="hinge"/>
    <geom friction="0.9" fromto="0 0 1.045 0 0 0.3" name="leg_geom" size="0.04" type="capsule
    "/>
    <body name="foot" pos="0.2 0 0">
      <joint axis="0 -1 0" name="foot_joint" pos="0 0 0.3" range="-45 45" type="hinge"/>
      <geom friction="0.9" fromto="-0.0 0 0.3 0.2 0 0.3" name="foot_geom" size="0.06" type="
      capsule"/>
    </body>
  </body>
</body>
```

Ant morphology shift : front ankle capsule size reduced by 20%

```
<geom fromto="0.0 0.0 0.0 0.1 0.1 0.0" name="left_ankle_geom" size="0.08" type="capsule"/>
<geom fromto="0.0 0.0 0.0 -0.1 0.1 0.0" name="right_ankle_geom" size="0.08" type="capsule"/>
```

HalfCheetah kinematic shift : back thigh joint range reduced by approximately 99%

```
<joint axis="0 1 0" damping="6" name="bthigh" pos="0 0 0" range="- .0052 .0105" stiffness
="240" type="hinge"/>
```

Hopper kinematic shift : thigh joint range reduced by 90%, foot joint range reduced by 60%

```
<joint axis="0 -1 0" name="thigh_joint" pos="0 0 1.05" range="-0.15 0" type="hinge"/>
<joint axis="0 -1 0" name="foot_joint" pos="0 0 0.1" range="-18 18" type="hinge"/>
```

Walker2d kinematic shift : foot joint range reduced by 99%

```
<joint axis="0 -1 0" name="foot_joint" pos="0 0 0.1" range="-0.45 0.45" type="hinge"/>
```

Ant kinematic shift : front hip joint ranges reduced by approximately 89%

```
<joint axis="0 0 1" name="hip_1" pos="0.0 0.0 0.0" range="-0.3 0.3" type="hinge"/>
<joint axis="0 0 1" name="hip_2" pos="0.0 0.0 0.0" range="-0.3 0.3" type="hinge"/>
```

Gravity shift : gravity magnitude reduced by 50%

```
<option gravity="0 0 -4.905" timestep="0.01"/>
```

Adroit kinematic shift (medium) : restricted index finger and thumb joints by 75%

```
<joint name="FFJ3" pos="0 0 0" axis="0 1 0" range="-0.109 0.109" user="1103"/>
<joint name="FFJ2" pos="0 0 0" axis="1 0 0" range="0 0.39275" user="1102"/>
<joint name="THJ4" pos="0 0 0" axis="0 0 -1" range="-0.26175 0.26175" user="1121"/>
<joint name="THJ0" pos="0 0 0" axis="0 1 0" range="-0.3925 0" user="1117"/>
```

Adroit kinematic shift (hard) : restricted index finger and thumb joints by 87.5%

```
<joint name="FFJ3" pos="0 0 0" axis="0 1 0" range="-0.0545 0.0545" user="1103"/>
<joint name="FFJ2" pos="0 0 0" axis="1 0 0" range="0 0.196375" user="1102"/>
<joint name="THJ4" pos="0 0 0" axis="0 0 -1" range="-0.130875 0.130875" user="1121"/>
<joint name="THJ0" pos="0 0 0" axis="0 1 0" range="-0.19625 0" user="1117"/>
```

Adroit morphology shift (medium) : finger phalanx half-lengths reduced to 50%

```
<geom name="C_ffproximal" class="DC_Hand" size="0.01 0.005625" pos="0 0 0.005625" type="capsule"/>
<geom name="C_ffmiddle" class="DC_Hand" size="0.00805 0.003125" pos="0 0 0.003125" type="capsule"/>
<geom name="C_ffdistal" class="DC_Hand" size="0.00705 0.003" pos="0 0 0.003" type="capsule"
condim="4"/>
```

Adroit morphology shift (hard) : finger phalanx half-lengths reduced to 25%

```
<geom name="C_ffproximal" class="DC_Hand" size="0.01 0.0028125" pos="0 0 0.0028125" type="capsule"/>
<geom name="C_ffmiddle" class="DC_Hand" size="0.00805 0.0015625" pos="0 0 0.0015625" type="capsule"/>
<geom name="C_ffdistal" class="DC_Hand" size="0.00705 0.0015" pos="0 0 0.0015" type="capsule"
condim="4"/>
```

### C.3 Hyperparameter Setup

We summarize the hyperparameters related to model training, data generation, and reinforcement learning in Table 8, and task-specific hyperparameters in Table 9.

For the coverage coefficient  $\lambda_{\text{cov}}$ , we set it to 0.1 for HalfCheetah and Walker2d under gravity shifts, as the target datasets in these domains often exhibit lower quality or form narrower distributions, making restricted coverage expansion preferable for maintaining high generation fidelity. For the remaining MuJoCo environments, we set  $\lambda_{\text{cov}} = 0.2$ . The policy regularization coefficient  $\beta$  is increased to 0.5 for Walker2d morphology shifts to enforce stronger adherence to the target behavior policy under large structural gaps. For the remaining MuJoCo environments, we use  $\beta = 0.001$ . For TCE(SM), the mixture coefficient  $\lambda_{\text{mix}}$  is set to 0.9 in HalfCheetah gravity shifts to leverage source samples when low-quality target data compromises generation accuracy. For the remaining MuJoCo environments, we set  $\lambda_{\text{mix}} = 0.1$  to prioritize target-aligned transitions while avoiding negative transfer from excessive source-data mixing. For Adroit tasks, we use the default parameter setup determined from the MuJoCo experiments, i.e.,  $\lambda_{\text{cov}} = 0.2$ ,  $\beta = 0.001$ , and  $\lambda_{\text{mix}} = 0.1$ .

Table 8: Shared hyperparameters for model training, sampling, and RL.

Category	Parameter Name	Value
Model Training	Learning rate	1e-4
	Optimizer	Adam
	Batch size	128
	Training epochs for $q_{\theta}^{\text{mix}}$	10K
	Training epochs for $q_{\theta}^{\text{tran}}$	5K
	Training epochs for $\text{Inv}_{\psi}, R_{\psi}$	1K
	Noise schedule $\alpha_{\text{min}}$	0.1
	Noise schedule $\alpha_{\text{max}}$	20
Sampling	Denoising steps $K$	500
RL Training	Learning rate for Actor, Critic	3e-4
	Optimizer for Actor, Critic	Adam
	Batch size for target sample	128
	Batch size for generated sample	128
	Training steps	1M

Table 9: Task-specific hyperparameters across different environments.

Parameter	Environment	Value
$\lambda_{\text{cov}}$	HalfCheetah, Walker2d (gravity shift)	0.1
	Other environments	0.2
$\lambda_{\text{mix}}$	HalfCheetah (gravity shift)	0.9
	Other environments	0.1
$\beta$	Walker2d (morphology shift)	0.5
	Other environments	0.001

## D Additional Performance Comparison

Section D.1 presents the full kinematic-shift results omitted from the main paper for space reasons. In Section D.2, we present performance comparisons in gravity shift environments not covered in the main paper. Section D.3 evaluates TCE under larger domain gaps using high-gravity settings from the ODRL benchmark [40]. Finally, Section D.4 reports comparative results against Meta-DT [29].

### D.1 Performance Comparison under Kinematic Shifts

Table 10 reports the full results for kinematic shifts. TCE continues to outperform prior cross-domain offline RL baselines on nearly all tasks, with TCE(OG) achieving the best overall average score. TCE(SM) remains competitive and occasionally performs better in milder cases, consistent with the main-text observation that limited source mixing can help as the domain gap decreases.

Table 10: Performance comparison in cross-domain offline RL under kinematic shifts.

Src.	Tgt.	IQL*	DARA	BOSA	SRPO	IGDF	OTDF	TCE(OG)	TCE(SM)
half-m	m	12.3±1.2	10.6±1.2	8.3±1.2	16.8±4.2	23.6±5.7	40.2±0.0	<b>42.2±2.4</b>	41.6±1.8
half-m	m-e	10.8±1.9	12.9±2.8	8.7±1.3	10.3±2.7	9.8±2.4	10.1±4.0	<b>40.7±2.7</b>	40.1±2.0
half-m	e	12.6±1.7	12.1±1.0	10.8±1.7	12.2±0.9	12.8±0.7	8.7±2.0	<b>21.3±0.8</b>	6.7±2.1
half-m-r	m	10.0±5.4	11.5±4.9	7.5±3.1	10.2±3.7	11.6±4.6	37.8±2.1	<b>42.0±0.2</b>	41.7±1.8
half-m-r	m-e	6.5±3.1	9.2±4.7	6.6±1.7	9.5±1.8	8.6±2.3	9.7±2.0	<b>41.6±0.5</b>	37.8±2.8
half-m-r	e	13.6±1.4	14.8±2.0	10.4±4.9	14.8±2.2	13.9±2.2	7.2±1.4	<b>23.4±1.5</b>	4.3±0.3
half-m-e	m	21.8±6.5	25.9±7.4	30.0±4.3	17.2±3.3	21.9±6.5	30.7±9.6	<b>41.9±0.3</b>	41.7±0.1
half-m-e	m-e	7.6±1.4	9.5±4.2	6.8±2.9	9.6±2.4	8.9±3.3	10.9±4.2	<b>40.0±2.5</b>	39.8±3.3
half-m-e	e	9.1±2.4	10.4±1.3	4.9±3.2	<b>11.2±1.0</b>	10.7±1.4	3.2±0.6	<b>11.2±1.2</b>	4.3±0.3
hopp-m	m	58.7±8.4	43.9±15.2	12.3±6.6	65.4±1.5	65.3±1.4	65.6±1.9	<b>66.0±0.4</b>	65.7±0.5
hopp-m	m-e	68.5±12.4	55.4±16.9	15.6±10.8	43.9±30.8	51.1±18.5	55.4±25.1	<b>75.7±2.2</b>	70.3±10.0
hopp-m	e	79.9±35.5	83.7±19.6	14.8±5.5	53.1±39.8	87.4±25.4	35.0±19.4	<b>91.5±5.7</b>	76.0±15.5
hopp-m-r	m	36.0±0.1	39.4±7.2	3.2±2.6	36.1±0.2	35.9±2.4	35.5±12.2	65.9±1.4	<b>66.2±0.2</b>
hopp-m-r	m-e	36.1±0.1	34.1±3.6	4.4±2.8	36.0±0.1	36.1±0.1	47.5±14.6	<b>82.8±4.3</b>	65.1±7.9
hopp-m-r	e	36.0±0.1	36.1±0.2	3.7±2.5	36.1±0.1	36.1±0.3	49.9±30.5	<b>84.8±7.0</b>	72.3±16.1
hopp-m-e	m	66.0±0.5	61.1±4.0	35.0±20.1	64.6±2.6	65.2±1.5	65.3±2.4	<b>67.3±0.8</b>	66.0±0.1
hopp-m-e	m-e	45.1±15.7	61.9±16.9	13.9±4.9	54.7±17.0	62.9±15.6	38.6±15.9	<b>74.7±8.9</b>	72.1±6.8
hopp-m-e	e	44.9±19.8	<b>84.2±21.1</b>	12.0±4.3	57.6±40.6	52.8±39.7	29.9±11.3	65.0±7.5	62.9±31.9
walk-m	m	34.3±9.8	35.2±22.5	14.3±11.2	39.0±6.7	41.9±11.2	49.6±18.0	<b>55.3±2.0</b>	53.5±7.7
walk-m	m-e	30.2±12.5	<b>51.9±11.5</b>	13.6±7.7	38.6±6.5	42.3±19.3	43.5±16.4	35.9±10.2	18.1±10.2
walk-m	e	56.4±18.2	40.7±14.4	15.3±2.5	57.3±12.2	60.4±17.5	46.7±13.6	<b>62.8±1.7</b>	38.7±15.3
walk-m-r	m	11.5±7.1	12.5±4.3	1.9±2.1	14.3±3.1	22.2±5.2	49.7±9.7	<b>55.6±9.5</b>	43.1±4.8
walk-m-r	m-e	9.7±3.8	11.2±5.0	4.6±3.0	4.2±5.1	7.6±4.9	<b>55.9±17.1</b>	40.9±10.0	47.2±10.3
walk-m-r	e	7.7±4.8	7.4±2.4	3.6±1.5	13.2±8.5	7.5±2.1	<b>51.9±7.9</b>	49.9±7.4	38.5±9.3
walk-m-e	m	41.8±8.8	38.1±14.4	21.4±8.3	36.9±4.3	41.2±13.0	44.6±6.0	46.3±5.4	<b>47.1±10.9</b>
walk-m-e	m-e	22.2±8.7	23.6±8.1	15.9±4.1	23.2±7.9	28.1±4.0	16.5±7.2	33.6±4.3	<b>38.3±10.5</b>
walk-m-e	e	26.3±10.4	36.0±9.2	18.5±3.6	40.9±9.6	46.2±19.4	42.4±9.1	<b>54.6±4.4</b>	42.5±5.7
ant-m	m	50.0±5.6	42.3±7.6	20.9±2.6	50.5±6.7	54.5±1.3	<b>55.4±0.0</b>	55.0±3.7	54.9±5.7
ant-m	m-e	57.8±7.2	54.1±3.8	31.7±7.0	54.9±1.3	54.5±4.6	60.7±3.6	<b>65.1±6.4</b>	61.8±1.0
ant-m	e	59.6±18.5	54.2±11.3	45.4±8.6	45.5±9.3	49.4±14.6	90.4±4.8	93.9±4.0	<b>94.3±1.8</b>
ant-m-r	m	43.7±4.6	42.0±5.4	19.0±1.8	45.3±5.1	41.4±5.0	52.8±4.4	<b>55.6±9.1</b>	54.1±4.2
ant-m-r	m-e	36.5±5.9	36.0±6.7	19.1±1.6	36.2±6.6	37.2±4.7	54.2±5.2	<b>65.6±5.4</b>	61.1±1.0
ant-m-r	e	24.4±4.8	22.1±0.4	19.5±0.8	27.1±3.7	24.3±2.8	74.7±10.5	92.3±3.7	<b>93.4±4.5</b>
ant-m-e	m	49.5±4.1	44.7±4.3	19.0±8.0	41.3±8.1	41.8±8.8	50.2±4.3	<b>57.2±2.7</b>	53.1±4.6
ant-m-e	m-e	37.2±2.0	33.3±7.0	6.4±2.5	38.2±8.0	41.5±4.9	48.8±2.7	<b>69.0±1.8</b>	59.4±10.5
ant-m-e	e	18.7±8.1	17.8±23.6	14.5±9.0	35.2±15.5	14.4±22.9	78.4±12.2	<b>97.3±1.3</b>	93.7±3.0
<b>Total Score</b>		1193.0	1219.8	513.5	1195.7	1271.0	1547.6	<b>2063.9</b>	1877.4

## D.2 Performance Comparison under Gravity Shifts

Table 11 reports the results for gravity shifts. All TCE variants outperform the baselines on most tasks, and TCE(SM) achieves the best overall average return. In HalfCheetah, where the target data is especially low-quality, the larger mixing ratio ( $\lambda_{\text{mix}} = 0.9$ ) improves stability and performance. Overall, the results support the same trend as in the main text: source mixing becomes more helpful when the shift is relatively mild.

Table 11: Performance comparison under gravity shifts.

Src.	Tgt.	IQL*	DARA	BOSA	SRPO	IGDF	OTDF	TCE(OG)	TCE(SM)
half-m	m	39.6±3.3	<b>41.2±3.9</b>	38.9±4.0	36.9±4.5	36.6±5.5	<u>40.7±7.7</u>	4.1±0.4	<u>40.7±1.2</u>
half-m	m-e	39.6±3.7	<b>40.7±2.8</b>	<u>40.4±3.0</u>	<b>40.7±2.3</b>	38.7±6.2	28.6±3.2	3.1±0.3	<u>39.2±0.5</u>
half-m	e	<b>42.4±3.8</b>	39.8±4.4	<u>40.5±3.9</u>	39.4±1.6	39.6±4.6	36.1±5.3	14.8±3.9	<u>41.1±6.1</u>
half-m-r	m	<u>20.1±5.0</u>	17.6±6.2	20.0±4.9	17.5±5.2	14.4±2.2	<b>21.5±6.5</b>	4.0±1.8	<u>18.1±7.2</u>
half-m-r	m-e	17.2±1.6	<u>20.2±5.2</u>	16.7±4.2	16.3±1.7	10.0±2.5	14.7±4.1	2.9±0.1	<b>20.3±5.1</b>
half-m-r	e	20.7±5.5	<u>22.4±1.7</u>	15.4±4.2	<b>23.1±4.0</b>	15.3±3.7	11.4±1.9	7.9±1.8	15.5±1.3
half-m-e	m	38.6±6.0	<u>37.8±3.3</u>	<u>41.8±5.1</u>	<b>42.5±2.3</b>	37.7±7.3	39.5±3.5	2.5±0.9	<u>39.4±2.7</u>
half-m-e	m-e	39.6±3.0	39.4±4.4	<u>38.7±2.7</u>	<b>43.3±2.7</b>	40.7±3.2	32.4±5.5	2.8±0.1	<u>41.3±4.5</u>
half-m-e	e	<u>43.4±0.9</u>	<b>45.3±1.3</b>	39.9±2.7	43.3±3.0	41.1±4.1	26.5±9.1	8.5±2.6	<u>41.7±1.4</u>
hopp-m	m	11.2±1.1	17.3±3.8	15.2±3.3	12.4±1.0	15.3±3.5	32.4±8.0	<b>61.9±2.7</b>	<u>52.5±4.7</u>
hopp-m	m-e	14.7±3.6	15.4±2.5	21.1±9.3	14.2±1.8	15.1±3.6	24.2±3.6	<b>46.2±2.6</b>	<u>35.0±7.9</u>
hopp-m	e	12.5±1.6	19.3±10.5	12.7±1.7	11.8±0.9	14.4±0.8	<u>33.7±7.8</u>	<b>53.4±2.2</b>	18.9±10.4
hopp-m-r	m	13.9±2.9	10.7±4.3	3.3±1.9	14.0±2.6	15.3±4.4	31.1±13.4	<b>60.7±2.7</b>	58.3±0.8
hopp-m-r	m-e	13.3±6.3	12.5±5.6	4.6±1.7	14.4±4.2	15.4±5.5	<u>24.2±6.1</u>	<u>24.2±3.1</u>	<b>32.7±10.4</b>
hopp-m-r	e	11.0±2.6	14.3±6.0	3.2±0.8	16.4±5.0	16.1±4.0	31.0±9.8	<b>73.4±7.8</b>	<u>55.7±15.0</u>
hopp-m-e	m	19.1±6.6	18.5±12.3	15.9±5.9	19.7±8.5	22.3±5.4	26.4±10.1	<b>61.3±5.6</b>	<u>54.0±5.8</u>
hopp-m-e	m-e	16.8±2.7	16.0±6.1	17.3±2.5	15.8±3.3	16.6±7.7	28.3±6.7	<b>45.5±9.8</b>	<u>33.4±7.2</u>
hopp-m-e	e	20.9±4.1	23.9±14.8	23.2±7.9	21.4±1.9	26.0±9.2	44.9±10.6	<b>66.3±5.8</b>	<u>55.8±8.3</u>
walk-m	m	28.1±12.9	28.4±13.7	<b>38.0±11.2</b>	21.4±7.0	22.1±8.4	<u>36.6±2.3</u>	36.3±0.9	<u>36.6±4.1</u>
walk-m	m-e	35.7±4.7	30.7±9.7	<u>40.9±7.2</u>	34.0±9.9	35.4±9.1	<b>44.8±7.5</b>	20.6±6.4	<u>40.9±6.0</u>
walk-m	e	37.3±8.0	36.0±7.0	<u>41.3±8.6</u>	39.5±3.8	36.2±13.6	<u>44.0±4.0</u>	20.3±1.6	<b>46.9±1.6</b>
walk-m-r	m	14.6±2.5	14.1±6.1	7.6±5.8	17.9±3.8	11.6±4.6	<u>32.7±7.0</u>	<b>35.8±0.8</b>	20.3±2.8
walk-m-r	m-e	15.3±1.9	15.9±5.8	4.8±5.8	15.3±4.5	13.9±6.5	<b>31.6±6.1</b>	<u>27.4±4.7</u>	18.2±1.6
walk-m-r	e	15.8±7.2	15.7±4.5	7.1±4.6	13.7±8.1	15.2±5.3	<b>31.3±5.3</b>	<u>21.5±2.9</u>	15.6±3.0
walk-m-e	m	39.9±13.1	41.6±13.0	32.3±7.2	<b>46.4±3.5</b>	33.8±3.1	30.2±9.8	33.0±2.1	<u>43.2±2.6</u>
walk-m-e	m-e	<u>49.1±6.9</u>	45.8±9.4	40.1±4.5	36.4±3.4	44.7±2.9	<b>53.3±7.1</b>	28.6±2.2	<u>45.6±1.7</u>
walk-m-e	e	40.4±11.9	56.4±3.5	43.7±4.4	45.8±8.0	45.3±10.4	61.1±3.4	31.6±4.9	<b>65.2±10.7</b>
ant-m	m	10.2±1.8	9.4±0.9	12.4±2.0	11.7±1.0	11.3±1.3	45.1±12.4	<b>57.0±6.1</b>	<u>56.4±5.1</u>
ant-m	m-e	9.4±1.2	10.0±0.9	11.6±1.3	10.2±1.2	9.4±1.4	33.9±5.4	<b>52.9±5.5</b>	<u>50.7±9.1</u>
ant-m	e	10.2±0.3	9.8±0.6	11.8±0.4	9.5±0.6	9.7±1.6	33.2±9.0	54.1±1.9	<b>55.7±6.4</b>
ant-m-r	m	18.9±2.6	21.7±2.1	13.9±1.5	18.7±1.7	19.6±1.0	29.6±10.7	<u>53.3±12.0</u>	<b>57.2±8.2</b>
ant-m-r	m-e	19.1±3.0	18.3±2.1	15.9±2.7	18.7±1.8	20.3±1.6	25.4±2.1	<u>42.4±10.9</u>	<b>44.0±11.6</b>
ant-m-r	e	18.5±0.9	20.0±1.3	14.5±1.7	19.9±2.1	18.8±2.1	24.5±2.8	<b>50.1±7.9</b>	40.5±13.9
ant-m-e	m	9.8±2.4	8.1±1.8	8.1±3.0	8.4±2.1	8.9±1.5	18.6±11.9	<b>58.0±11.7</b>	<u>53.8±10.4</u>
ant-m-e	m-e	9.0±0.8	6.4±1.4	6.2±1.5	6.1±3.5	7.2±2.9	34.0±9.4	<b>46.0±10.3</b>	<u>43.8±6.1</u>
ant-m-e	e	9.1±2.6	10.4±2.9	4.2±3.9	8.8±1.0	9.2±1.5	23.2±2.9	<b>58.0±3.7</b>	<u>45.7±18.9</u>
<b>Total Score</b>		825.0	851.0	763.2	825.5	803.6	1160.7	<u>1270.4</u>	<b>1473.9</b>

### D.3 Performance Comparison under Extreme Domain Shifts

To investigate the robustness of our method under extreme dynamics mismatches, we conduct experiments on Ant tasks with a severe gravity shift, increasing gravitational acceleration by a factor of 5 (from  $-9.81 \text{ m/s}^2$  to  $-49.05 \text{ m/s}^2$ ), following the protocol of ODRL [40]. Such drastic alteration in physical parameters exacerbates the domain gap, rendering the source policy nearly ineffective in the target environment. As summarized in Table 12, TCE(OG) significantly outperforms both the baselines and TCE(SM) across all dataset configurations. Crucially, we observe a distinct shift in the efficacy of source mixing compared to the standard gravity setting reported in Table 11: while TCE(SM) typically benefits from retrieving source transitions when the gap is mild, TCE(OG) proves superior in this extreme regime. This result corroborates our analysis that when the dynamics gap is substantial, relying on source data can induce negative transfer due to large kinematic discrepancies. Consequently, TCE(OG) achieves robust performance by strictly utilizing target-consistent generated transitions, thereby effectively mitigating the impact of severe physical perturbations.

Table 12: Performance comparison on extreme gravity-shift tasks.

Src.	Tgt.	IQL*	OTDF	TCE(OG)	TCE(SM)
ant-m	m	31.9±0.2	34.5±0.2	<b>70.8±0.5</b>	64.7±2.8
ant-m	e	31.3±0.3	38.2±3.1	<b>86.9±0.8</b>	49.3±8.9
ant-m-r	m	18.6±0.2	24.8±0.4	<b>44.3±1.6</b>	41.1±6.5
ant-m-r	e	18.6±0.1	23.1±1.2	<b>70.9±5.5</b>	23.9±1.8
ant-m-e	m	30.1±0.0	35.0±0.9	<b>70.1±1.2</b>	68.6±5.7
ant-m-e	e	31.6±0.1	33.7±1.1	<b>82.5±0.4</b>	56.0±6.7
<b>Total Score</b>		162.1	189.3	<b>425.5</b>	303.6

#### D.4 Comparison with Additional Baselines

We additionally compare TCE against Meta-DT\* [29] and DmC [22]. Meta-DT\* is a representative meta-offline RL approach adapted for our setting by training on the union of source and target datasets, while DmC is a recent diffusion-based method that generates additional source-domain data. As shown in Table 13, Meta-DT\* significantly underperforms compared to TCE and even falls short of IQL\* in many tasks. This performance gap highlights a fundamental difference in objectives: meta-offline RL aims to generalize across diverse tasks, whereas cross-domain offline RL focuses on bridging the specific distribution shift between source and target domains. Without a mechanism to explicitly align domains or selectively transfer relevant source knowledge, meta-learning approaches struggle to overcome large domain gaps in a zero-shot manner, confirming the necessity of our targeted domain adaptation strategy. Meanwhile, TCE generally outperforms DmC across a majority of tasks, attributable to our strategy of directly synthesizing target-aligned transitions rather than source-like data, thereby reducing the domain gap more effectively. We note that since the official code for DmC is unavailable, we report the performance directly from the original paper.

Table 13: Performance comparison of TCE with Meta-DT\* and DmC under kinematic shifts

Src.	Tgt.	IQL*	Meta-DT*	DmC	OTDF	TCE(OG)	TCE(SM)
half-m	m	12.3±1.2	13.4 ± 3.4	38.5±1.4	40.2±0.0	<b>42.2±2.4</b>	41.6±1.8
half-m	m-e	10.8±1.9	8.5±0.6	19.1±1.0	10.1±4.0	<b>40.7±2.7</b>	40.1±2.0
half-m	e	12.6±1.7	5.0±0.1	13.1±0.8	8.7±2.0	<b>21.3±0.8</b>	6.7±2.1
half-m-r	m	10.0±5.4	5.5±0.7	19.5±1.8	37.8±2.1	<b>42.0±0.2</b>	41.7±1.8
half-m-r	m-e	6.5±3.1	7.5±1.1	11.4±2.1	9.7±2.0	<b>41.6±0.5</b>	37.8±2.8
half-m-r	e	13.6±1.4	6.4±2.8	15.6±2.9	7.2±1.4	<b>23.4±1.5</b>	4.3±0.3
half-m-e	m	21.8±6.5	4.7±0.2	38.4±1.4	30.7±9.6	<b>41.9±0.3</b>	41.7±0.1
half-m-e	m-e	7.6±1.4	7.7±3.2	24.1±4.6	10.9±4.2	<b>40.0±2.5</b>	39.8±3.3
half-m-e	e	9.1±2.4	2.8±0.2	<b>13.4±2.0</b>	3.2±0.6	11.2±1.2	4.3±0.3
hopp-m	m	58.7±8.4	5.0±0.2	<b>69.8±2.3</b>	65.6±1.9	66.0±0.4	65.7±0.5
hopp-m	m-e	68.5±12.4	4.9±0.2	<b>78.2±5.1</b>	55.4±25.1	75.7±2.2	70.3±10.0
hopp-m	e	79.9±35.5	5.2 ± 0.2	59.8±21.8	35.0±19.4	<b>91.5±5.7</b>	76.0±15.5
hopp-m-r	m	36.0±0.1	36.4± 0.2	64.8±2.4	35.5±12.2	65.9±1.4	<b>66.2±0.2</b>
hopp-m-r	m-e	36.1±0.1	36.3± 0.1	69.7±7.5	47.5±14.6	<b>82.8±4.3</b>	65.1±7.9
hopp-m-r	e	36.0±0.1	37.6± 0.1	69.9±18.0	49.9±30.5	<b>84.8±7.0</b>	72.3±16.1
hopp-m-e	m	66.0±0.5	3.5± 0.4	<b>69.6±1.3</b>	65.3±2.4	67.3±0.8	66.0±0.1
hopp-m-e	m-e	45.1±15.7	8.5± 2.3	<b>75.5±9.6</b>	38.6±15.9	74.7±8.9	72.1±6.8
hopp-m-e	e	44.9±19.8	6.4±0.2	64.5±24.2	29.9±11.3	<b>65.0±7.5</b>	62.9±31.9
walk-m	m	34.3±9.8	5.0±0.3	<b>63.2±4.2</b>	49.6±18.0	55.3±2.0	53.5±7.7
walk-m	m-e	30.2±12.5	15.7±2.0	<b>53.5±7.0</b>	43.5±16.4	35.9±10.2	18.1±10.2
walk-m	e	56.4±18.2	10.0±0.9	<b>70.5±12.0</b>	46.7±13.6	62.8±1.7	38.7±15.3
walk-m-r	m	11.5±7.1	3.4±1.0	52.9±8.4	49.7±9.7	<b>55.6±9.5</b>	43.1±4.8
walk-m-r	m-e	9.7±3.8	14.6±0.1	36.4±5.4	<b>55.9±17.1</b>	40.9±10.0	47.2±10.3
walk-m-r	e	7.7±4.8	8.9±1.0	44.4±8.5	<b>51.9±7.9</b>	49.9±7.4	38.5±9.3
walk-m-e	m	41.8±8.8	8.5±0.8	<b>59.4±6.8</b>	44.6±6.0	46.3±5.4	47.1±10.9
walk-m-e	m-e	22.2±8.7	10.2±8.7	<b>53.2±7.3</b>	16.5±7.2	33.6±4.3	38.3±10.5
walk-m-e	e	26.3±10.4	5.7±2.6	<b>69.2±7.0</b>	42.4±9.1	54.6±4.4	42.5±5.7
ant-m	m	50.0±5.6	13.9±0.7	<b>62.1±0.6</b>	55.4±0.0	55.0±3.7	54.9±5.7
ant-m	m-e	57.8±7.2	14.8±0.3	<b>68.9±1.0</b>	60.7±3.6	65.1±6.4	61.8±1.0
ant-m	e	59.6±18.5	14.9±0.1	92.1±3.5	90.4±4.8	93.9±4.0	<b>94.3±1.8</b>
ant-m-r	m	43.7±4.6	22.3±0.2	<b>61.9±0.5</b>	52.8±4.4	55.6±9.1	54.1±4.2
ant-m-r	m-e	36.5±5.9	21.0±0.1	58.8±3.6	54.2±5.2	<b>65.6±5.4</b>	61.1±1.0
ant-m-r	e	24.4±4.8	26.8±2.2	43.8±2.6	74.7±10.5	92.3±3.7	<b>93.4±4.5</b>
ant-m-e	m	49.5±4.1	13.5±0.1	<b>60.6±1.3</b>	50.2±4.3	57.2±2.7	53.1±4.6
ant-m-e	m-e	37.2±2.0	13.6±0.1	60.4±3.7	48.8±2.7	<b>69.0±1.8</b>	59.4±10.5
ant-m-e	e	18.7±8.1	18.1±1.2	76.0±4.1	78.4±12.2	<b>97.3±1.3</b>	93.7±3.0
<b>Total Score</b>		1193.0	446.2	1902.2	1547.6	<b>2063.9</b>	1877.4

## E Error Analysis on Additional Environments

To further demonstrate the robustness of our method, we analyze the quality of generated samples on HalfCheetah and Hopper environments (morphology shift, medium-to-expert) with respect to the coverage bound  $\lambda_{cov}$ . We evaluate the approximation fidelity of the accepted transitions against ground-truth dynamics using three metrics: action reconstruction error, reward prediction error, and transition dynamics error.

**HalfCheetah.** A trend similar to that reported in the error analysis of Section 5 is also found in HalfCheetah tasks, as shown in Fig. 7. Although the overall error scale remains relatively small compared to the Ant environment, we confirm a consistent pattern where errors accumulate as coverage expands. Fig. 7(a)–(c) illustrate this monotonic increase in action, reward, and transition errors with higher  $\lambda_{cov}$ . These results further validate the importance of restricting  $\lambda_{cov}$  to a reliable range to ensure that the augmented data remains physically plausible.

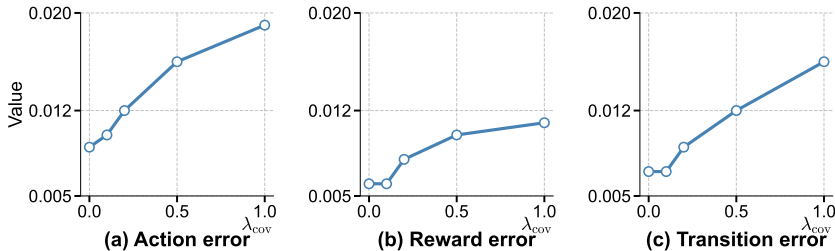


Figure 7: Sample reliability with respect to  $\lambda_{cov}$  in HalfCheetah morphology shifts.

**Hopper.** Fig. 8 illustrates the error trends in Hopper tasks as the coverage bound relaxes. We observe that Hopper exhibits a notably drastic increase in approximation errors as coverage expands. Specifically, Fig. 8(a) demonstrates a significant spike in action reconstruction error at higher  $\lambda_{cov}$ , while Fig. 8(b)–(c) confirm a correspondingly steep rise in reward and transition errors. This acute sensitivity underscores that, given a substantial domain gap, restricting  $\lambda_{cov}$  to a low range is critical to prevent the inclusion of unreliable transitions that could destabilize learning.

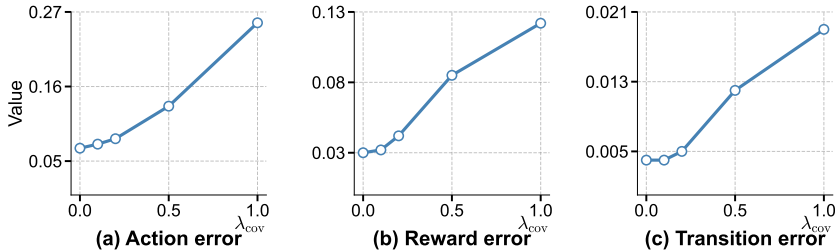


Figure 8: Sample reliability with respect to  $\lambda_{cov}$  in Hopper morphology shifts.

## F Computational Complexity

This section compares the computational resources required by IQL\* [12], OTDF [15], and TCE on morphology shift (medium-to-expert) tasks. Experiments were conducted on a server with AMD EPYC 7513 CPUs and NVIDIA RTX 3090 GPUs. Note that TCE(OG) and TCE(SM) share identical costs due to their shared architecture. While all methods require approximately three hours for the common offline RL phase, OTDF adds roughly 18 minutes for data selection. TCE incurs approximately 48 minutes for score network training and 16 minutes for sampling; these costs remain consistent across tasks, with only marginal increases for higher-dimensional environments like Ant. Crucially, because the score modeling, sampling, and RL phases are executed sequentially with intermediate memory deallocation, TCE maintains a constant peak GPU memory usage of roughly 2 GB, imposing marginal overhead compared to the baseline. As summarized in Table 14, the modest computational cost is justified by the substantial performance gains.

Table 14: Comprehensive runtime and memory usage comparison averaged over 36 morphology shift tasks. Note that GPU memory usage represents the peak allocation during the entire pipeline.

Method	Model Training	Data Sampling	Offline RL	Peak GPU Memory
IQL*	–	–	3h	2 GB
OTDF	–	18 min	3h	2 GB
TCE	48m	16m	3h	2 GB

## G Additional Analysis

This section presents detailed analysis not covered in the main text. Section G.1 provides the ablation results for the coverage coefficient  $\lambda_{cov}$  and the mixture coefficient  $\lambda_{mix}$ . Section G.2 analyzes the effect of target data size on inverse-dynamics error and policy performance. Section G.3 analyzes the sensitivity to the denoising step  $K$ .

### G.1 Ablation Studies on $\lambda_{cov}$ and $\lambda_{mix}$

**Coverage Coefficient  $\lambda_{cov}$ .** The coverage coefficient  $\lambda_{cov}$  controls the trade-off between expanding state coverage and maintaining proximity to the target distribution. Fig. 9 illustrates the performance trends across different values of  $\lambda_{cov}$  under morphology, kinematic, and gravity shifts on the Ant task (medium-replay-to-medium-expert). As shown, the performance remains relatively stable across a wide range, generally outperforming the simple augmentation baseline. However, we observe a slight performance degradation as  $\lambda_{cov}$  increases to 0.5. This aligns with our analysis in Section 5 that overly aggressive coverage expansion introduces transitions with higher approximation errors. Therefore, we suggest prioritizing sample fidelity by selecting  $\lambda_{cov}$  from a conservative range. Larger values are best reserved for scenarios where the target dataset is extremely sparse, necessitating broader exploration even at the cost of slight dynamics mismatch.

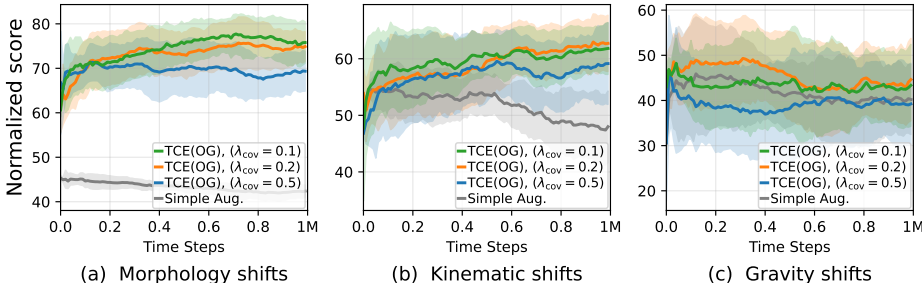


Figure 9: Performance sensitivity to  $\lambda_{cov}$  across different domain shifts on the Ant medium-replay-to-medium-expert task.

**Mixture Coefficient  $\lambda_{\text{mix}}$ .** The mixture coefficient  $\lambda_{\text{mix}}$  regulates the ratio of source transitions directly incorporated into the training set, balancing data abundance against distribution shift. Fig. 10 illustrates the impact of  $\lambda_{\text{mix}}$  across different domain shifts. We observe that lower values (0 or 0.1) generally yield stable performance. Notably, in scenarios like gravity shifts, a mild mixture TCE(SM) ( $\lambda_{\text{mix}} = 0.1$ ) outperforms TCE(OG) ( $\lambda_{\text{mix}} = 0$ ), while further increasing  $\lambda_{\text{mix}}$  leads to a sharp performance drop. Based on these results, we conclude that setting  $\lambda_{\text{mix}} = 0$  provides the most robust baseline in the presence of distinct structural disparities. However, a small positive coefficient can be advantageous when source and target dynamics are closely aligned or when the target dataset quality is low. In the latter case, high generation errors may compromise the reliability of synthesized transitions, making the inclusion of real source data a beneficial strategy to stabilize learning. Conversely, excessive mixing biases the generative model toward source transitions, introducing significant dynamics mismatch that outweighs the benefits of data augmentation.

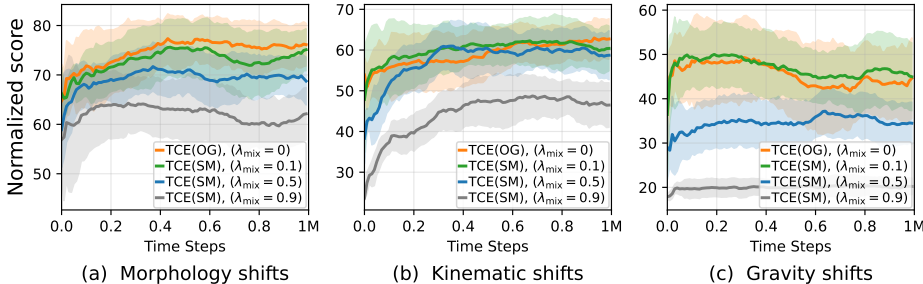


Figure 10: Performance sensitivity to  $\lambda_{\text{mix}}$  across different domain shifts on the Ant medium-replay-to-medium-expert task.

## G.2 Effect of Target Data Size on Inverse Dynamics Error

We further evaluate how reducing the target-data size affects the inverse dynamics model and downstream policy performance. Our main setting already uses only 5K target transitions, roughly five episodes, yet the error analysis in the main text shows that the inverse-dynamics prediction error remains small. To stress this regime further, we vary the target-data size from 2K to 20K transitions and report the resulting action prediction error and normalized score in Table 15. As expected, reducing the target data to 2K increases the inverse-dynamics error and slightly lowers performance, but the method remains strong. As the target-data size increases, the error decreases and the performance improves accordingly.

Table 15: Action prediction error and normalized score under different target-data sizes.

Metric	2K	5K (ours)	10K	20K
Action error	0.142±0.018	0.065±0.012	0.042±0.009	<b>0.015±0.006</b>
Score	90.3±4.2	94.0±4.5	94.4±3.8	<b>95.0±3.1</b>

### G.3 Ablation Study on Denoising Step $K$

We examine the sensitivity of TCE to the denoising step hyperparameter  $K$ , which governs the trade-off between sampling computational cost and generation quality by determining the discretization granularity of the reverse process. Table 16 presents the results of TCE(OG) on the Ant morphology-shift environment across  $K \in \{100, 200, 500\}$ , using  $K = 500$  as the default configuration. While  $K = 500$  generally yields the highest average scores, the performance differences across varying  $K$  values are minimal and mostly fall within the standard deviation ranges. This result demonstrates that TCE is not highly sensitive to the choice of  $K$ , ensuring robust performance without the need for precise hyperparameter tuning.

Table 16: Performance of TCE(OG) on Ant morphology-shift tasks at different  $K$  values.

Src.	Tgt.	K=100	K=200	K=500
ant-m	m	<b>42.2±1.8</b>	42.0±0.28	41.5±0.8
ant-m	m-e	72.5±2.3	<b>74.1±0.50</b>	72.7±2.5
ant-m	e	91.9±0.1	<u>92.8±2.8</u>	<b>94.0±4.5</b>
ant-m-r	m	40.7±1.2	<u>40.8±0.71</u>	<b>41.5±1.5</b>
ant-m-r	m-e	<u>70.0±2.8</u>	69.2±3.1	<b>71.0±8.4</b>
ant-m-r	e	<u>90.8±1.6</u>	<u>91.3±3.8</u>	<b>96.1±0.3</b>
ant-m-e	m	41.4±0.9	41.2±0.6	<b>41.9±0.6</b>
ant-m-e	m-e	<b>66.5±3.1</b>	66.1±1.6	<u>66.4±1.2</u>
ant-m-e	e	93.7±0.5	<u>94.0±1.1</u>	<b>96.6±0.5</b>
Total Score		609.7	<u>611.5</u>	<b>621.7</b>

## H Broader Impact

Target-aligned Coverage Expansion (TCE) improves cross-domain offline reinforcement learning when target-domain data is scarce and additional online interaction is infeasible. In domains such as robotics and other safety- or cost-sensitive settings, this can reduce the burden of target-domain data collection while improving the practicality of offline adaptation.

At the same time, unreliable transfer under large source-target mismatch may still lead to incorrect policy behavior after deployment, especially if generated transitions are over-trusted. These risks should be mitigated through careful validation, conservative deployment, and continued robustness and safety evaluation.

## NeurIPS Paper Checklist

### 1. Claims

Question: Do the main claims made in the abstract and introduction accurately reflect the paper’s contributions and scope?

Answer: [Yes]

Justification: *The paper’s main claims are stated in the abstract and introduction.*

Guidelines:

- The answer [N/A] means that the abstract and introduction do not include the claims made in the paper.
- The abstract and/or introduction should clearly state the claims made, including the contributions made in the paper and important assumptions and limitations. A [No] or [N/A] answer to this question will not be perceived well by the reviewers.
- The claims made should match theoretical and experimental results, and reflect how much the results can be expected to generalize to other settings.
- It is fine to include aspirational goals as motivation as long as it is clear that these goals are not attained by the paper.

### 2. Limitations

Question: Does the paper discuss the limitations of the work performed by the authors?

Answer: [Yes]

Justification: *The main limitations of the approach are discussed in a dedicated section.*

Guidelines:

- The answer [N/A] means that the paper has no limitation while the answer [No] means that the paper has limitations, but those are not discussed in the paper.
- The authors are encouraged to create a separate “Limitations” section in their paper.
- The paper should point out any strong assumptions and how robust the results are to violations of these assumptions (e.g., independence assumptions, noiseless settings, model well-specification, asymptotic approximations only holding locally). The authors should reflect on how these assumptions might be violated in practice and what the implications would be.
- The authors should reflect on the scope of the claims made, e.g., if the approach was only tested on a few datasets or with a few runs. In general, empirical results often depend on implicit assumptions, which should be articulated.
- The authors should reflect on the factors that influence the performance of the approach. For example, a facial recognition algorithm may perform poorly when image resolution is low or images are taken in low lighting. Or a speech-to-text system might not be used reliably to provide closed captions for online lectures because it fails to handle technical jargon.
- The authors should discuss the computational efficiency of the proposed algorithms and how they scale with dataset size.
- If applicable, the authors should discuss possible limitations of their approach to address problems of privacy and fairness.
- While the authors might fear that complete honesty about limitations might be used by reviewers as grounds for rejection, a worse outcome might be that reviewers discover limitations that aren’t acknowledged in the paper. The authors should use their best judgment and recognize that individual actions in favor of transparency play an important role in developing norms that preserve the integrity of the community. Reviewers will be specifically instructed to not penalize honesty concerning limitations.

### 3. Theory assumptions and proofs

Question: For each theoretical result, does the paper provide the full set of assumptions and a complete (and correct) proof?

Answer: [Yes]

Justification: *For the theoretical results, we state the assumptions and provide complete proofs.*

Guidelines:

- The answer [N/A] means that the paper does not include theoretical results.
- All the theorems, formulas, and proofs in the paper should be numbered and cross-referenced.
- All assumptions should be clearly stated or referenced in the statement of any theorems.
- The proofs can either appear in the main paper or the supplemental material, but if they appear in the supplemental material, the authors are encouraged to provide a short proof sketch to provide intuition.
- Inversely, any informal proof provided in the core of the paper should be complemented by formal proofs provided in appendix or supplemental material.
- Theorems and Lemmas that the proof relies upon should be properly referenced.

#### 4. Experimental result reproducibility

Question: Does the paper fully disclose all the information needed to reproduce the main experimental results of the paper to the extent that it affects the main claims and/or conclusions of the paper (regardless of whether the code and data are provided or not)?

Answer: [Yes]

Justification: *The paper includes the information needed to reproduce the experiments, and the code will be released.*

Guidelines:

- The answer [N/A] means that the paper does not include experiments.
- If the paper includes experiments, a [No] answer to this question will not be perceived well by the reviewers: Making the paper reproducible is important, regardless of whether the code and data are provided or not.
- If the contribution is a dataset and/or model, the authors should describe the steps taken to make their results reproducible or verifiable.
- Depending on the contribution, reproducibility can be accomplished in various ways. For example, if the contribution is a novel architecture, describing the architecture fully might suffice, or if the contribution is a specific model and empirical evaluation, it may be necessary to either make it possible for others to replicate the model with the same dataset, or provide access to the model. In general, releasing code and data is often one good way to accomplish this, but reproducibility can also be provided via detailed instructions for how to replicate the results, access to a hosted model (e.g., in the case of a large language model), releasing of a model checkpoint, or other means that are appropriate to the research performed.
- While NeurIPS does not require releasing code, the conference does require all submissions to provide some reasonable avenue for reproducibility, which may depend on the nature of the contribution. For example
  - (a) If the contribution is primarily a new algorithm, the paper should make it clear how to reproduce that algorithm.
  - (b) If the contribution is primarily a new model architecture, the paper should describe the architecture clearly and fully.
  - (c) If the contribution is a new model (e.g., a large language model), then there should either be a way to access this model for reproducing the results or a way to reproduce the model (e.g., with an open-source dataset or instructions for how to construct the dataset).
  - (d) We recognize that reproducibility may be tricky in some cases, in which case authors are welcome to describe the particular way they provide for reproducibility. In the case of closed-source models, it may be that access to the model is limited in some way (e.g., to registered users), but it should be possible for other researchers to have some path to reproducing or verifying the results.

#### 5. Open access to data and code

Question: Does the paper provide open access to the data and code, with sufficient instructions to faithfully reproduce the main experimental results, as described in supplemental material?

Answer: [Yes]

Justification: *Our code and data will be released together with instructions to reproduce the main results.*

Guidelines:

- The answer [N/A] means that paper does not include experiments requiring code.
- Please see the NeurIPS code and data submission guidelines (<https://neurips.cc/public/guides/CodeSubmissionPolicy>) for more details.
- While we encourage the release of code and data, we understand that this might not be possible, so [No] is an acceptable answer. Papers cannot be rejected simply for not including code, unless this is central to the contribution (e.g., for a new open-source benchmark).
- The instructions should contain the exact command and environment needed to run to reproduce the results. See the NeurIPS code and data submission guidelines (<https://neurips.cc/public/guides/CodeSubmissionPolicy>) for more details.
- The authors should provide instructions on data access and preparation, including how to access the raw data, preprocessed data, intermediate data, and generated data, etc.
- The authors should provide scripts to reproduce all experimental results for the new proposed method and baselines. If only a subset of experiments are reproducible, they should state which ones are omitted from the script and why.
- At submission time, to preserve anonymity, the authors should release anonymized versions (if applicable).
- Providing as much information as possible in supplemental material (appended to the paper) is recommended, but including URLs to data and code is permitted.

## 6. Experimental setting/details

Question: Does the paper specify all the training and test details (e.g., data splits, hyperparameters, how they were chosen, type of optimizer) necessary to understand the results?

Answer: [Yes]

Justification: *Experimental details are specified in the main paper and appendix.*

Guidelines:

- The answer [N/A] means that the paper does not include experiments.
- The experimental setting should be presented in the core of the paper to a level of detail that is necessary to appreciate the results and make sense of them.
- The full details can be provided either with the code, in appendix, or as supplemental material.

## 7. Experiment statistical significance

Question: Does the paper report error bars suitably and correctly defined or other appropriate information about the statistical significance of the experiments?

Answer: [Yes]

Justification: *For the main results, we report standard errors over multiple runs and describe how they are computed.*

Guidelines:

- The answer [N/A] means that the paper does not include experiments.
- The authors should answer [Yes] if the results are accompanied by error bars, confidence intervals, or statistical significance tests, at least for the experiments that support the main claims of the paper.
- The factors of variability that the error bars are capturing should be clearly stated (for example, train/test split, initialization, random drawing of some parameter, or overall run with given experimental conditions).

- The method for calculating the error bars should be explained (closed form formula, call to a library function, bootstrap, etc.)
- The assumptions made should be given (e.g., Normally distributed errors).
- It should be clear whether the error bar is the standard deviation or the standard error of the mean.
- It is OK to report 1-sigma error bars, but one should state it. The authors should preferably report a 2-sigma error bar than state that they have a 96% CI, if the hypothesis of Normality of errors is not verified.
- For asymmetric distributions, the authors should be careful not to show in tables or figures symmetric error bars that would yield results that are out of range (e.g., negative error rates).
- If error bars are reported in tables or plots, the authors should explain in the text how they were calculated and reference the corresponding figures or tables in the text.

#### 8. Experiments compute resources

Question: For each experiment, does the paper provide sufficient information on the computer resources (type of compute workers, memory, time of execution) needed to reproduce the experiments?

Answer: [Yes]

Justification: *We specify the compute resources for all experiments, including hardware type and runtime, in the appendix.*

Guidelines:

- The answer [N/A] means that the paper does not include experiments.
- The paper should indicate the type of compute workers CPU or GPU, internal cluster, or cloud provider, including relevant memory and storage.
- The paper should provide the amount of compute required for each of the individual experimental runs as well as estimate the total compute.
- The paper should disclose whether the full research project required more compute than the experiments reported in the paper (e.g., preliminary or failed experiments that didn't make it into the paper).

#### 9. Code of ethics

Question: Does the research conducted in the paper conform, in every respect, with the NeurIPS Code of Ethics <https://neurips.cc/public/EthicsGuidelines>?

Answer: [Yes]

Justification: *Our research fully conforms to the NeurIPS Code of Ethics.*

Guidelines:

- The answer [N/A] means that the authors have not reviewed the NeurIPS Code of Ethics.
- If the authors answer [No], they should explain the special circumstances that require a deviation from the Code of Ethics.
- The authors should make sure to preserve anonymity (e.g., if there is a special consideration due to laws or regulations in their jurisdiction).

#### 10. Broader impacts

Question: Does the paper discuss both potential positive societal impacts and negative societal impacts of the work performed?

Answer: [Yes]

Justification: *We discuss both positive and negative societal impacts in the Broader Impact section of the appendix.*

Guidelines:

- The answer [N/A] means that there is no societal impact of the work performed.
- If the authors answer [N/A] or [No], they should explain why their work has no societal impact or why the paper does not address societal impact.

- Examples of negative societal impacts include potential malicious or unintended uses (e.g., disinformation, generating fake profiles, surveillance), fairness considerations (e.g., deployment of technologies that could make decisions that unfairly impact specific groups), privacy considerations, and security considerations.
- The conference expects that many papers will be foundational research and not tied to particular applications, let alone deployments. However, if there is a direct path to any negative applications, the authors should point it out. For example, it is legitimate to point out that an improvement in the quality of generative models could be used to generate Deepfakes for disinformation. On the other hand, it is not needed to point out that a generic algorithm for optimizing neural networks could enable people to train models that generate Deepfakes faster.
- The authors should consider possible harms that could arise when the technology is being used as intended and functioning correctly, harms that could arise when the technology is being used as intended but gives incorrect results, and harms following from (intentional or unintentional) misuse of the technology.
- If there are negative societal impacts, the authors could also discuss possible mitigation strategies (e.g., gated release of models, providing defenses in addition to attacks, mechanisms for monitoring misuse, mechanisms to monitor how a system learns from feedback over time, improving the efficiency and accessibility of ML).

## 11. Safeguards

Question: Does the paper describe safeguards that have been put in place for responsible release of data or models that have a high risk for misuse (e.g., pre-trained language models, image generators, or scraped datasets)?

Answer: [N/A]

Justification: *The study uses only open-source simulators and does not involve releasing data or models with elevated misuse risk.*

Guidelines:

- The answer [N/A] means that the paper poses no such risks.
- Released models that have a high risk for misuse or dual-use should be released with necessary safeguards to allow for controlled use of the model, for example by requiring that users adhere to usage guidelines or restrictions to access the model or implementing safety filters.
- Datasets that have been scraped from the Internet could pose safety risks. The authors should describe how they avoided releasing unsafe images.
- We recognize that providing effective safeguards is challenging, and many papers do not require this, but we encourage authors to take this into account and make a best faith effort.

## 12. Licenses for existing assets

Question: Are the creators or original owners of assets (e.g., code, data, models), used in the paper, properly credited and are the license and terms of use explicitly mentioned and properly respected?

Answer: [Yes]

Justification: *All simulation environments used in the paper are open-source, and their original sources are properly credited.*

Guidelines:

- The answer [N/A] means that the paper does not use existing assets.
- The authors should cite the original paper that produced the code package or dataset.
- The authors should state which version of the asset is used and, if possible, include a URL.
- The name of the license (e.g., CC-BY 4.0) should be included for each asset.
- For scraped data from a particular source (e.g., website), the copyright and terms of service of that source should be provided.

- If assets are released, the license, copyright information, and terms of use in the package should be provided. For popular datasets, [paperswithcode.com/datasets](https://paperswithcode.com/datasets) has curated licenses for some datasets. Their licensing guide can help determine the license of a dataset.
- For existing datasets that are re-packaged, both the original license and the license of the derived asset (if it has changed) should be provided.
- If this information is not available online, the authors are encouraged to reach out to the asset's creators.

### 13. **New assets**

Question: Are new assets introduced in the paper well documented and is the documentation provided alongside the assets?

Answer: [Yes]

Justification: *A source-code package and usage guide accompany the paper, and the code will be publicly released to facilitate reproducibility and benchmarking.*

Guidelines:

- The answer [N/A] means that the paper does not release new assets.
- Researchers should communicate the details of the dataset/code/model as part of their submissions via structured templates. This includes details about training, license, limitations, etc.
- The paper should discuss whether and how consent was obtained from people whose asset is used.
- At submission time, remember to anonymize your assets (if applicable). You can either create an anonymized URL or include an anonymized zip file.

### 14. **Crowdsourcing and research with human subjects**

Question: For crowdsourcing experiments and research with human subjects, does the paper include the full text of instructions given to participants and screenshots, if applicable, as well as details about compensation (if any)?

Answer: [N/A]

Justification: *The work does not involve crowdsourcing or any research with human subjects.*

Guidelines:

- The answer [N/A] means that the paper does not involve crowdsourcing nor research with human subjects.
- Including this information in the supplemental material is fine, but if the main contribution of the paper involves human subjects, then as much detail as possible should be included in the main paper.
- According to the NeurIPS Code of Ethics, workers involved in data collection, curation, or other labor should be paid at least the minimum wage in the country of the data collector.

### 15. **Institutional review board (IRB) approvals or equivalent for research with human subjects**

Question: Does the paper describe potential risks incurred by study participants, whether such risks were disclosed to the subjects, and whether Institutional Review Board (IRB) approvals (or an equivalent approval/review based on the requirements of your country or institution) were obtained?

Answer: [N/A]

Justification: *Because the study does not involve human subjects, IRB approval is not applicable.*

Guidelines:

- The answer [N/A] means that the paper does not involve crowdsourcing nor research with human subjects.

- Depending on the country in which research is conducted, IRB approval (or equivalent) may be required for any human subjects research. If you obtained IRB approval, you should clearly state this in the paper.
- We recognize that the procedures for this may vary significantly between institutions and locations, and we expect authors to adhere to the NeurIPS Code of Ethics and the guidelines for their institution.
- For initial submissions, do not include any information that would break anonymity (if applicable), such as the institution conducting the review.

#### 16. **Declaration of LLM usage**

Question: Does the paper describe the usage of LLMs if it is an important, original, or non-standard component of the core methods in this research? Note that if the LLM is used only for writing, editing, or formatting purposes and does not impact the core methodology, scientific rigor, or originality of the research, declaration is not required.

Answer: [N/A]

Justification: *No large language models were used as important, original, or non-standard components in the core methods of this research.*

Guidelines:

- The answer [N/A] means that the core method development in this research does not involve LLMs as any important, original, or non-standard components.
- Please refer to our LLM policy in the NeurIPS handbook for what should or should not be described.